New generation of magnetic and luminescent nanoparticles for in-vivo real-time imaging

Lise-Marie Lacroix, Fabien Delpech, Céline Nayral, Sébastien Lachaize, Bruno Chaudret

New generation of magnetic and luminescent nanoparticles for *in-vivo* real-time imaging.

Lise-Marie Lacroix,* Fabien Delpech,* Céline Nayral, Sébastien Lachaize, Bruno Chaudret

Université de Toulouse, INSA, UPS, LPCNO (Laboratoire de Physique et Chimie des Nano-Objets), F-31077 Toulouse, France; CNRS; UMR 5215 ; LPCNO, F-31077 Toulouse, France

Summary :

A new generation of optimized contrast agents is emerging, based on metallic nanoparticles (NPs) and semiconductor nanocrystals (NCs) for respectively magnetic resonant imaging (MRI) and near-infra-red (NIR) fluorescent imaging techniques. Compared with established contrast agents such as iron oxide NPs or organic dyes, these NPs benefit from several advantages: their magnetic and optical properties can be tuned through size, shape and composition engineering, their efficiency can excess by several order of magnitude that one of contrast agents clinically used, their surface can be modified to incorporate specific targeting agents and antifolding polymers to increase the blood circulation time and the tumor recognition, they can possibly be integrated in complex architecture to yield multimodal imaging agents. In this review, we will report the materials of choice based on the understanding of the physics basics of NIR and MRI techniques and their corresponding syntheses as NPs. Surface engineering, water transfer, and specific targeting will be highlighted prior to their first use for *in-vivo* real-time imaging. Highly efficient NPs, safer in use and target specific are likely to be entering clinical applications in a near future.

Key index words : Contrast agents, MRI, Near-Infra Red, luminescent nanocrystals, quantum dots, core-shell

Since the discovery, by chance, of X-ray potentiality by Roentgen in 1896, imaging techniques have been optimized and extended. Depending on the penetration depth, the spatial resolution and the sensitivity required, X-ray computed tomography (CT), Positron Emission Tomography (PET), Magnetic Resonance Imaging (MRI) or optical imaging, such as Near-Infrared (NIR) fluorescent imaging, may be selected as the most relevant imaging modality [1]. In all cases, enhancement of the signal over noise ratio, and thus of the sensitivity of these imaging techniques, requires the introduction of contrast agents such as radioisotopes, paramagnetic molecules or more recently inorganic nanoparticles [2]. The latter have benefited from tremendous advances during the last two decades notably in terms of available synthetic routes. In particular, the improvements of the solution-phase approaches allow now an easy and low-cost access (compared to classical physical or vacuum methods) to well-controlled nano-probes. Prominent examples of imaging modalities which have profited from this intense research activity are MRI and NIR luminescence: a new generation of sophisticated nano-objects has reached such stage of maturity, especially in terms of probe sensitivity, that their use has on one hand, become a standard practice in *in vitro* biology research and on the other hand, hold promise for *in-vivo* real-time detection.

This review intends to highlight these advances and developments that occurred in the last few years for MRI and NIR luminescence detection. In the case of MRI, the upgrading of contrast agents based on oxide NPs to metallic NPs yields to strongly enhanced probe sensitivity. As will be detailed herein, this was achieved thanks (i) to the unprecedented magnetization related on metallic nature of the NPs and (ii) to the narrow size distribution allowing homogeneous and intense magnetic properties from one NP to another. Similarly, in the case of NIR, impressive progress has been realized on the synthesis of quantum dots (QDs) able to absorb and emit efficiently in the NIR range of wavelength (where the transmissivity of organic tissue is maximum). Additionally, following the trend toward

"greener" chemistry, new versions of QDs free of Cd, Pb and Hg are now available. These significant advances have motivated this review dedicated to an up-to-date perspective on magnetic NPs and NIR emitting QDs. Moreover, because of different features in terms of sensitivity, resolution, acquisition time and operational costs, fluorescence-based *in vivo* imaging techniques are complementary to MRI.[1] NIR enables faster measurements with higher sensitivity. [1, 3, 4] while MRI ensures a higher spatial resolution and depth of penetration. Thus, very recent work focused on bimodal NPs, *i.e.* combining MRI and NIR modalities, will also be addressed as challenging perspective in view of designing more and more sensitive probes and/or multifunctional theranostic nano-objects (MRI contrast agents can also be used as heating centers in magnetic hyperthermia).[5]

After a general introduction on liquid phase synthesis of NPs, we will present the basics of MRI and the general chemical synthesis for new generation of optimized contrast agents. Near infra-red fluorescence technique requirements will then be discussed, optimal material being highlighted. Corresponding type-I and type-II quantum dots synthesis will be listed. MRI and NIR contrast agents being prepared mostly in organic solvants, we will review the surface engineering strategies to ensure the water-transfer of generic inorganic NPs and their further biodistribution and specific targeting. Up-to-date results of real time in-vivo MRI and NIR imaging obtained with new generation of NPs will be reviewed before concluding on the requirements and first promising attempt for NIR/MRI multifunctional NPs.

I. Liquid-phase synthesis of inorganic NPs

This brief part aims at introducing the general principles of NPs synthesis in solution to give the reader the keys to a deep understanding of the numerous synthesis examples presented hereafter (parts II.2 and III.2). This review focuses on the chemical approach to NPs

formation particularly because of its ability to provide NPs samples (i) of high quality and (ii) in adequate amounts for further biological use.

Colloidal solutions of nanoparticles of various natures (metallic, semi-conducting, oxides) can be prepared by chemical approach. The general strategy followed relies on the decomposition of a precursor, typically a salt or an organometallic compound (Figure 1). This decomposition yield free atoms which tend to aggregate to form small seeds during the nucleation step. Metallic NP synthesis may require the use of a reducing agent to convert oxidized atoms (M^{n+}) into metallic atoms (M^0). The seeds formed during the nucleation step then grow by successive addition of atoms, by coalescence or through a ripening based process [6, 7]. To prevent NPs from aggregation and sintering, organic molecules (surfactants) or polymers are added to ensure steric hindrance or electrostatic repulsion between NPs.

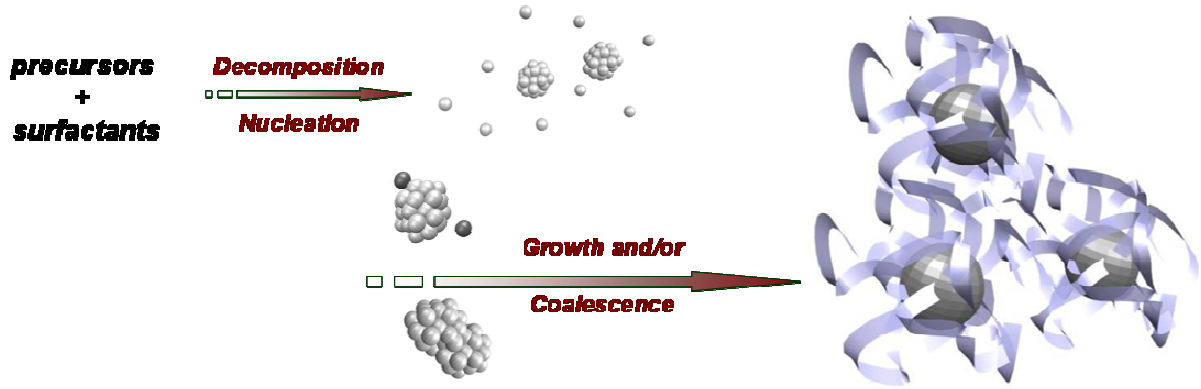

Figure 1. Schematic view of the general mechanism driving chemical NP synthesis.

Since physical properties depend on the size, size distribution and shape of NPs, nucleation and growth steps must be carefully tuned. Monodisperse NPs (with a narrow size distribution $\sigma < 10\%$) could be prepared via a burst nucleation, fast and limited in time, followed by a homogeneous growth [8]. Nucleation and growth steps extent depends of

experimental parameters such as reaction time, temperature, nature of the precursors and surfactants, thus careful optimization of these parameters are usually required. [9]

II. MRI principle and nanomaterials:

In this section we will first introduce the basics of MRI, highlighting the requirements for optimized contrast agents : (i) high magnetization materials, (ii) large magnetic core size, and (iii) core accessibility to water protons. Up-to-date syntheses of magnetic nanoparticles will then be reviewed in the context of *in vivo* MRI imaging i.e. (i) metallic material preferred to oxides due to their enhanced magnetization and (ii) narrow-size distribution to ensure homogeneity of the magnetic properties.

II.1 Basics of MRI:

Clinical MRI is based on the relaxation of the nuclear spin of water protons in a strong magnetic field (1.5T to 3T in hospitals, 9T or greater in laboratories). Into such static field B_0, spins tend to align parallel or antiparallel (Figure 2a), and precess at the Larmor frequency ω_0 which is propotional to the field strength:

$$\omega_0 = B_0.\gamma \quad \text{(Eq. 1)}$$

where γ is the gyromagnetic ratio (for hydrogen, $\gamma = 42{,}6$ MHz/T)

Once magnetized by the static field, protons can be excited through a perpendicular pulsed field B_1 (rotating around the B_0 axis at the Larmor frequency, i.e. in the radio frequency range RF), which leads to a magnetization M_{xy} that is perpendicularly to B_0 (Figure 2b). After the removal of the RF field, spins tend to realign with B_0 following (Figure 2): a longitudinal

relaxation (M_Z increasing according to an exponential law, time constant T_1, Figure 2d), and a transverse relaxation (exponential decay of M_{xy}, time constant T_2, Figure 2e).

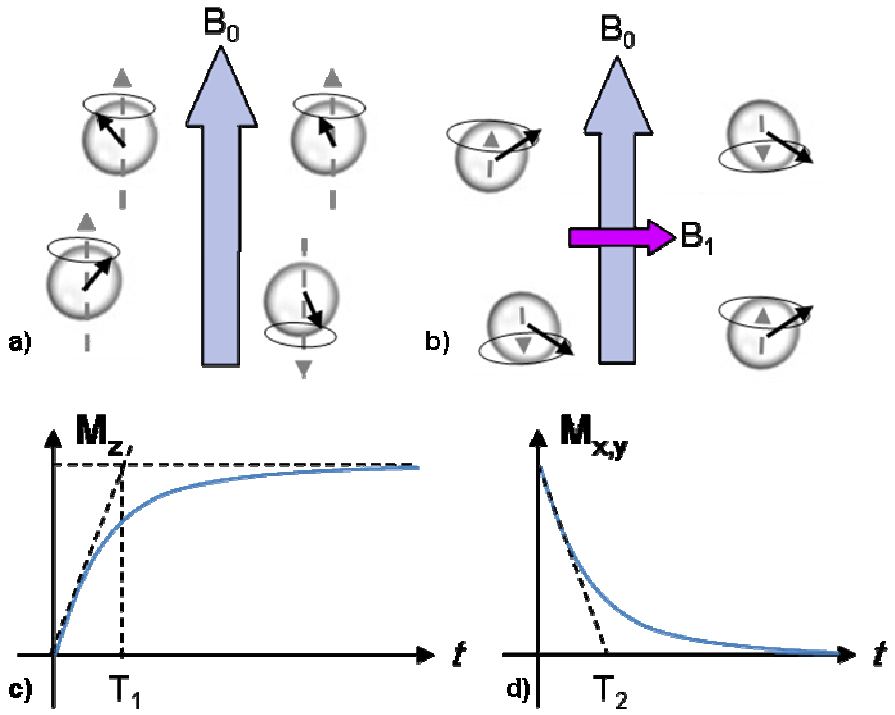

Figure 2. Schematic view of water proton spins in a) a static magnetic field B_0 and b) upon RF-excitation Dashed arrow represents M_Z component, solid circle represents $M_{X,Y}$ component. Evolution as a function of time of d)M_Z and e) $M_{X,Y}$ with respectively T_1 and T2 as time constant derived from the initial slope (dashed lines).

MR images are acquired while protons return to their equilibrium state, contrast being based on the difference of relaxation rate $R_i=1/T_i$ (i=1 or 2). Relaxation rate depends of numerous parameters among which the surrounding medium, field strength, temperature, accessibility of protons and of course nature of the contrast agents. Intrinsiquelly, tumor cells exhibit different relaxation constants compared to healthy surrounding tissues, which can lead to an MRI contrast. However, dedicated cancer imaging may require an enhancement of the signal over noise ratio.

Static magnetic field applied can be increased to accelerate the precession of spins (Eq. 1) and to slightly improve the excess proportion of spins aligned parallel (low energy state). Signal being linked with the relative magnetization of tissues, i.e. the spin excess,

enhancement could be reached. However, establishing large homogeneous field on whole body is not technologically easy, thus improvement of signal at fixed magnetic field strength (up to 3T), through the introduction of adequate contrast agents, is still required.

Paramagnetic, superparamagnetic or ferromagnetic contrast agents affect both relaxation processes [10]. However, depending of their nature, they will increase more specifically the relaxation rate R_1 (positive contrast agent) or R_2 (negative contrast agent). Paramagnetic ions (mainly Gadolinium(III) complexes) have been widely used as positive contrast agents in clinical applications. [11,12,13] However, high dose of these toxic metal ions are required due to the relatively low efficiency of Gd-based contrast agents. Nanoparticles, among which iron oxides NPs, have received lots of interest as efficient non toxic R_2 contrast agents for the last 20 years. [14]

Magnetic nanoparticles are small magnets which generate a magnetic field at their vicinity (Figure 3). Such field inhomogeneity accelerates the phase decoherence of the spins [15]. Therefore, NPs act as negative contrast agents, their efficiency being quantified through the normalized relaxativity $r_2=R_2/\text{concentration}$ ($mMol^{-1}s^{-1}$). In first approximation, relaxativity varies as the square of the magnetic field induced at the vicinity of the water proton. The magnetic field is a short-distance perturbation, which vanishes quickly:

$$r \propto d^{-6}.(M_S V)^2 \qquad \text{(Eq. 2)}$$

where d is the distance proton-center of the magnetic NP, M_S is the saturation magnetization and V the volume.

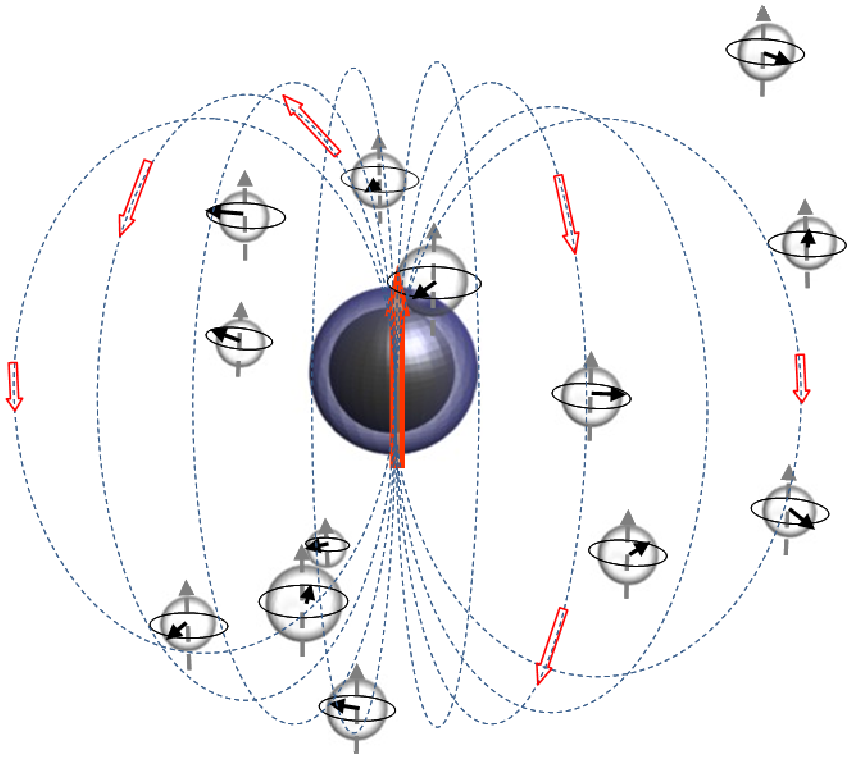

Figure 3. Schematic view of a magnetic nanoparticle surrounded by water protons. Red arrow indicate the magnetic field induced.

The accessibility of the water proton to the NP surface is of particular importance due to the d^{-6} decrease of r. Therefore, from a magnetic point of view, the coating of magnetic core, which ensure the biostability of the inorganic NPs as described in section 3, should be as thin as possible to yield high relaxativity (Table 1). However, biostability often requires relatively large coating, as discussed in section 3, thus, a delicate balance should be found regarding the corona shell thickness.

In order to improve the relaxativity, larger NPs could also be used [16, 17] (Table 1), but size affects the magnetic behaviour of nanoparticles. At small size (below 12 nm for Fe), NPs behave as paramagnetic species (superparamagnetism): they can be easily magnetized under B_0 and do not exhibit magnetization in absence of magnetic field (remnant state Mr=0). At larger size, NPs are ferromagnetic and exhibit a net magnetization (Mr≠ 0). This difference of behaviour affects the stability of NPs in solution through the modification of dipolar interactions (in first approximation α Mr^2 [18]). Aggregation of the ferrofluid may arise for

ferromagnetic NPs, thus, superparamagnetic NPs have been prevailing materials so far for in vivo applications. Recently, larger NPs with peculiar magnetic configuration (vortex state), have been proposed for bioapplications [19]. These NPs exhibit a very low magnetization in absence of any applied field (weak Mr), resulting in weak interparticle interactions, but a large volume and thus a presumably high relaxativity. Such vortex states are observed for intermediate size range, typically 30 – 100 nm for iron [20, 21].

In addition to the size control, one could optimize M_S. Saturation magnetization is an intrinsic parameter of the material chosen and corresponds to the maximum magnetic moment that can be reached upon an applied field. Magnetic dopants, such as Mn, can be added to ferrite materials, leading to a slight increase of M_S (Table 1). To further enhance M_S, metals, such as Fe or Co, should be preferred to their oxide counterparts (Table 1). Though contrast agents used clinically are nowadays only based on SPION (superparamagnetic iron oxide nanoparticles) [22], the design of optimized contrast agents would benefit from metallic NPs, providing that these NPs do not exhibit toxicity [23]. Thus, we will focus our discussion on the recent strategies developed to synthesize and protect metallic nanoparticles with optimized properties.

Material	M_S (emu/g_{metal})	Core size (nm)	Magnetic state	Organic corona		r_2 ($s^{-1}.mM^{-1}$)	B_0 (T)	Ref
				Ligand	Size (nm)			
CLIO-Fe_xO_y	-	-	-			62		[24]
Fe_3O_4	101	12	-	DMSA	2	218	1.5	[24]
	-	10	-	PEG PEI -	7	40	1.5	[25]
	-	10	-	PEI	2	75	1.5	[25]
$MnFe_2O_4$	~60	6	-	DMSA	2	208	1.5	[24]
	~90	9	-	DMSA	2	265	1.5	[24]
	110	12	-	DMSA	2	358	1.5	[24]
$Fe@Fe_3O_4$	70	10	FM	PEG	2	129	1.5	[26]
	140	16	FM	DMSA	2	324	9.4	[27]
	112	15	FM	PEG	15	67	3	[28]
	164	15	FM	PEG	15	220	3	[28]
Co@Au	-	30-90	-		-	10^7	7	[29]

FeCo@C	162	4	SPM	PEG	17	185	1.5	[30]
	215	7	SPM	PEG	17	644	1.5	[30]
FePt	125	9	SPM	TMAOH	2	239	4.7	[31]

Table 1. r_2 relaxativities of magnetic NPs. CLIO : cross linked iron oxide NPs, used in clinical applications. SPM : superparamagnetic; FM: ferromagnetic; DMSA : 2,3-dimercaptosuccinic acid ; PEG : polyethylenglycol; TMAOH : tetramethylammonium hydroxide

II.2 Synthesis of Magnetic NPs

Multiple strategies have been developed to synthesize monodispersed iron oxide nanoparticles (maghemite γ-Fe_2O_3 or magnetite Fe_3O_4), either in aqueous [32] or in organic solvents.[33] Size control could be reached by the decomposition of organometallic precursors at high temperature in presence of long alkyl chain surfactants [34, 35], further synthesis information being found in recent review articles.[36, 37] Concerning magnetic dopants, they can be added in the spinel structure by co-reduction at high temperature of organometallic precursors such as $Mn(acac)_2$ and $Fe(acac)_3$. [38]

Here, we will focus our attention on synthesis of metallic NPs, promising higher magnetization, as explained previously. Iron being highly reactive towards oxidation, metallic Fe NPs were mainly prepared in organic solvents (Table 2) [39]. Classicaly, $Fe(CO)_5$ was decomposed at high temperature in presence of long-chain amine [40, 41]. Though highly toxic, this precursor benefited from Fe atoms already reduced (oxidation degree 0), therefore no reducing agent were required. However, the magnetic properties of the NPs obtained were generally lower than the bulk value, due to their intrinsic carburation from CO byproduct [42]. To prevent such carburation, $Fe(CO)_5$ can be replaced by iron salts or organometallic compounds whose decomposition did not yield any carbon source. Due to their high stability, the decomposition and reduction of iron salts required harsh conditions. For instance, $FeCl_2$

could be reduced in water by sodium borohydride, but boron contamination has been found to decrease the NP moment [26]. Therefore, decomposition of organometallic compounds such as $Fe(C_5H_5)(C_6H_7)$ [27] or $\{Fe[N(SiMe_3)_2]_2\}_2$ [43,44] under dihydrogen atmosphere could be preferred to yield unoxidized iron NPs in mild conditions (bulk magnetization). Due to its high reactivity, the latter amido precursor could also be reduced solely by a long chain amine in absence of H_2 [45]. The optimization of the nucleation and growth steps, through the tuning of experimental parameters (temperature, surfactants), yielded Fe NPs with unprecedent size and shape control in the range 1 to 100 nm (Figure 4a-b).

Cobalt NPs can be prepared following similar procedures. $Co_2(CO)_8$ could be decomposed at high temperature to yield monodisperse NPs [46,47]. As observed for Fe, the binding of –CO species at the NPs' surface decreased their magnetic properties [48]. Cobalt salt ($CoCl_2$) could be reduced with strong reducing agent (superhydride $LiEt_3BH$) but yield NPs with ε-Co crystalline phase with degraded magnetic properties prior to annealing treatment [49]. Co can crystallize in hexagonal compact (hcp) structure which exhibit optimized magnetic properties. Benefiting from the crystallographic unicity of the c axis, intensive researches have been devoted to the synthesis of anisotropic Co NPs. Polyol synthesis [50] as long as organometallic approaches [51,52] yielded single crystalline Co nanorods with a relatively narrow size distribution (Figure 4c). Though nanorods have never been tested for MRI purposes, they could potentially present high relaxativity, analogously to elongated Co@Au nanowonton, prepared through physical process [29]. (Table 1)

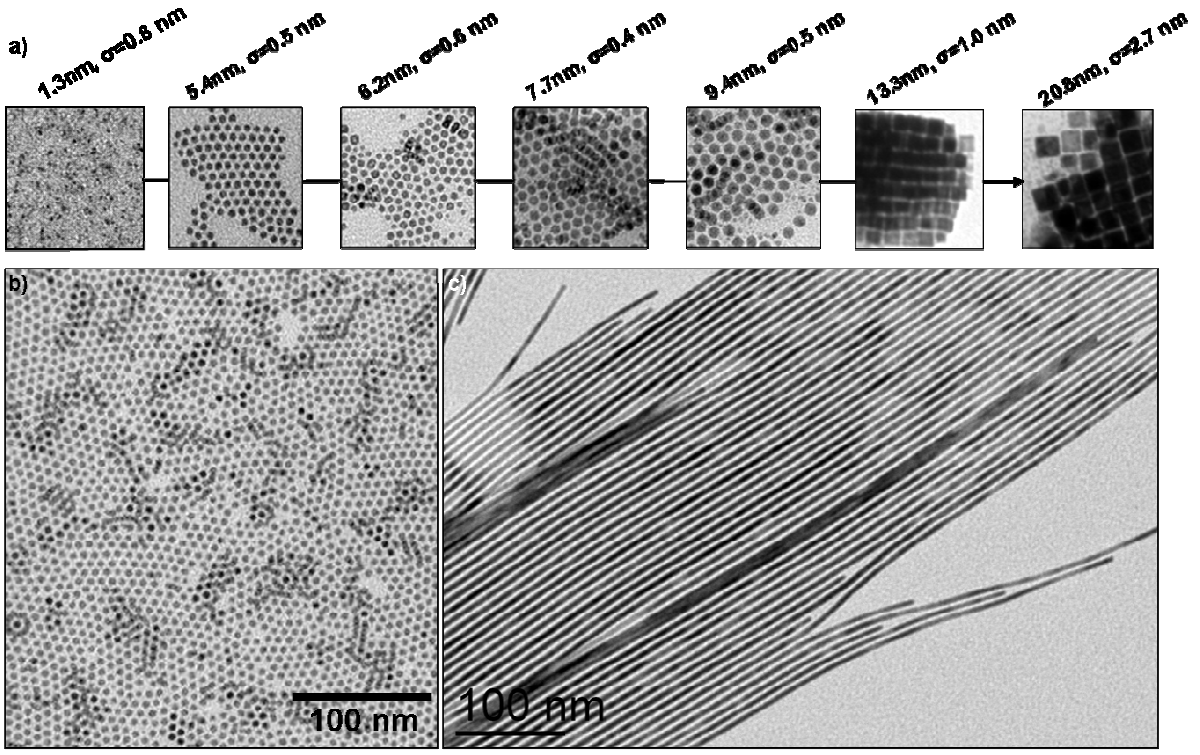

Figure 4. Transmission electron microscope (TEM) micrographs of a-b) Fe NPs with tuneable mean size. Reprinted with permission from [53] c) Co nanorods obtained by decomposition under H_2. Reprinted with permission from [52] Copyright 2012. American Chemical Society

To further enhance the magnetic moment, Fe or Co could be replaced by FeCo NPs, providing that highly crystalline NPs with optimized composition (60% Fe, 40% Co) could be prepared. However, the synthesis has been very challenging due to the difference of reactivity of Fe and Co precursors, yielding core-shell structure (Co@Fe) with reduced magnetic properties [54]. In order to favour the interdiffusion of Fe and Co, annealing treatments (from 250°C [55,56] to 500°C [54]) were performed, yielding bcc-FeCo NPs with saturation magnetization up to 220 emu/g_{FeCo} [54]. Though chemically prepared FeCo NPs have never been tested for MRI purposes, high T_1 and T_2 relaxativities without any obvious cytotoxicity could be expected as reported for bcc-FeCo NPs prepared via an arc-discharge method. [30] Lately, Pt-based alloys (FePt, CoPt) have also been investigated for biomedical applications. Initially developed for magnetic recording purposes due to the high magnetic anisotropy of tetragonally ordered structures ($L_1$0-phase) [57], FePt combines an enhanced magnetization

compared to iron oxides (125 emu/g_{FePt} [58]) and a high cytotoxicity, making them potent anticancer drug due to the leaching of Pt ions in biological condition. [59]

Material	Precursor	Method	Surfactants	T (°C)	Core size (nm)	M_S (emu/g_{metal})	Ref
Fe	$Fe(CO)_5$	Thermodecomposition	OA+OY OA HDAHCl-OY	287 285 180	6-11 7-35 15	132-200 - 164	[41] [60] [28]
	$Fe(oleate)_3$	Thermodecomposition	OA+NaOA	310	16	101	[61]
	$(Fe(N(Si(CH_3)_3)_2)_2)_2$	Reduction - H_2	PA+HDA LA+DDA	150 150	1-30 30-80	212 210	[44] [21]
	$Fe(C_5H_5)(C_6H_7)$	Reduction - H_2	OA	130	16	140	[27]
	$FeCl_2$	Reduction – $LiEt_3BH$ Reduction – $NaBH_4$	PMMA PEG	20 20	5-25 10	85-184 70	[62] [26]
Co	$Co_2(CO)_8$	Thermodecomposition	OA+TOPO	180	10-16	-	[46]
	$CoCl_2$	Reduction – $LiEt_3BH$	OA+TOP	200	2-11	-	[49]
	$Co(laurate)_2$	Polyol	-	170	10*100	113	[50]
	$Co(N(Si(CH_3)_3)_2)_2(thf)$	Reduction - H_2	LA+HDA	150	13,7	-	[52]
	$Co(\eta_3-C_8H_{13})(\eta_4-C_8H_{12})$	Reduction - H_2	SA+HDA	150	9*40	142	[51]
FeCo	$Co_2(CO)_8 + Fe(CO)_5$	Thermodecomposition Interdiffusion Co/Fe	OY OA+OY+DOA	160 – 250	11 11	212 192	[56] [55]
	$Co(\eta_3-C_8H_{13})(\eta_4-C_8H_{12})+Fe(CO)_5$	Thermodecomposition +Reduction - H_2	OA+SA+HDA	150 – 500	15	220	[54]
	$Co(acac)_2 + Fe(acac)_3$	Reduction - H_2 Diol	OA+OY	300	20	207	[63]
FePt	$Pt(acac)_2 + Fe(CO)_5$	Thermodecomposition + Reduction Diol	OA+OY	297	6	-	[57]
	$Pt(acac)_2+Fe(acac)_3$	Polyol	HDD	295	2	-	[64]
	$Pt(acac)_2 + FeCl_2$	Reduction – $LiBEt_3H$	OA+OY	263	4	75	[65]

Table 2. Overview of the chemical approaches for the synthesis of metallic NPs. OA: oleic acid. OY: oleylamine. HDAHCl: hexadecylamonium chloride. NaOA : sodium oleate. PA: palmitic acid. HDA: hexadecylamine. LA: lauric acid. DDA: dodecylamine. PMMA: polymethylmethacrylate. PEG: polyethyleneglycol. TOP: trioctylphosphine. TOPO: trioctylphosphine oxide. DOA: dioctylamine. SA: Stearic acid

III. NIR detection principle and NIR luminescent semiconductor nanocrystals:

In this section, we will first present the basis of NIR imaging and in particular the relevancy (i) of the NIR wavelength window for a high signal to background ratio (thanks to the high

transmissivity of the organic tissue in this range of wavelengths) and (ii) of the QDs compared to other fluorescent probes. Then, we will focus on the existing synthetic routes with an emphasis on the development of non-toxic semiconductor nanocrystals (NCs) as alternative to Cd-, Pb- and Hg- based QDs. These approaches will be examined in the context of preparing NCs well-suited for *in vivo* imaging i.e. (i) small size to facilitate circulation and clearance and, (ii) narrow-size distribution and brightness to provide efficient detection at QDs concentration as low as possible.

III.1 Basics of NIR luminescence imaging

Context

Among the various modalities for bioimaging, fluorescence imaging is of special interest because of its low cost, high sensitivity, high spatial resolution and ease to implement (just with a low light camera). In the case of real time *in vivo* detection, the fundamental barriers to fluorescence imaging of a tissue are auto-fluorescence, high light scattering and absorption of the different tissue and blood components: water, haemoglobin, melanin, proteins…(Figure 5).[66]

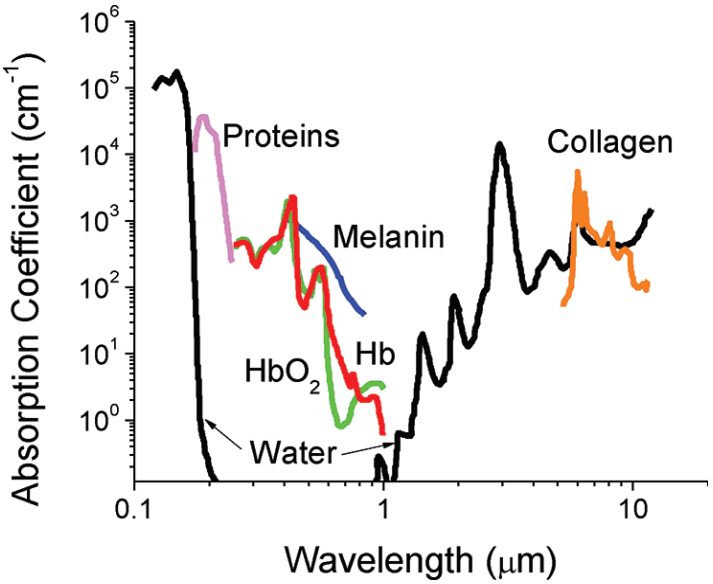

Figure 5: Absorbance of various tissue and blood components from 200 nm to 10 μm. Reprinted with permission from [66] Copyright 2012. American Chemical Society.

These endogenous absorbers possess high absorption characteristics between 200-650 nm and thus, prevent light to penetrate deep into the tissues in the visible range. Moreover, the tissue auto-fluorescence also limits the signal-to-background ratio and hampers the detection of the fluorescent imaging agent. These intrinsic limitations have stimulated, in the last few years, the development of fluorescent probes with absorption and emission maxima in the 650-1450 nm range where tissues have minimal absorbance and fluorescence.[66,67, 68]

As a general guideline, ideal fluorescent probes should fulfil also the following requirements [69] :

- Stability in biological media.
- Long fluorescence lifetimes for an efficient temporal discrimination from scattered excitation light.
- High brightness (product of high quantum yield, i.e. high number of emitted photons per number of absorbed photons, and high extinction coefficient).
- Narrow, symmetric emission bands and large Stokes shifts to easily separate the excitation and emission.
- No toxicity or interference with cell physiology.

The organic fluorescent dyes (cyanines, pyrroles- or porphyrins-based cycles, squaraines and borondipyrromethene classes) [66] which were historically first used in NIR biodetection,[70] are far away to be ideal probes. In the far-red/near-infrared (NIR) wavelengths range, they suffer from rather low quantum yield, photobleaching (making them unsuitable for extended period of observation) and broad emission spectra which create overlapping detection ranges (inadequate for simultaneous multicolor applications).[66,71] Even if remarkable progresses have been made to improve the performances of dye-doped silica NPs and to develop new

probes such as up-converting NPs [72,73] or noble metal (gold and silver) nanoclusters, [**Erreur ! Signet non défini.**, 74] the optical performances (especially QYs) are not yet competitive enough.

Among the NIR fluorescent probes, [**Erreur ! Signet non défini.**] quantum dots (QDs) offer today the best optical properties and appear as a very powerful and essential tool in biodetection. Indeed, they exhibit large molar extinction coefficients, high QY (> 50%), narrow and symmetric photoluminescence (PL) emission bands, size-tunable emission and absorption spectra, large two-photon action cross-section, and high photostability.[69] However, QDs suffer from the drawback of blinking (intermittence in light emission), which is problematic in case of single molecule tracking [75], instability of QY in different media and possible emission variability do to slight size modification between chemical batches.

QDs specificities

Owing to their nanoscale dimension, the intrinsic physical characteristics of the material are transformed by quantum effect below a certain size limit (Bohr radius) which ranges from ~2 nm to ~50 nm according to the material.[76] At these sizes, nanocrystals lie in between the atomic and molecular limit (discrete density of electronic levels) and the extended crystalline limit (continuous bands i.e. the valence band and the conduction band) of bulk semiconductor. This leads to size-dependent optical properties (Figure 6),[77] the maximum emission wavelength attainable being that of the bulk material.

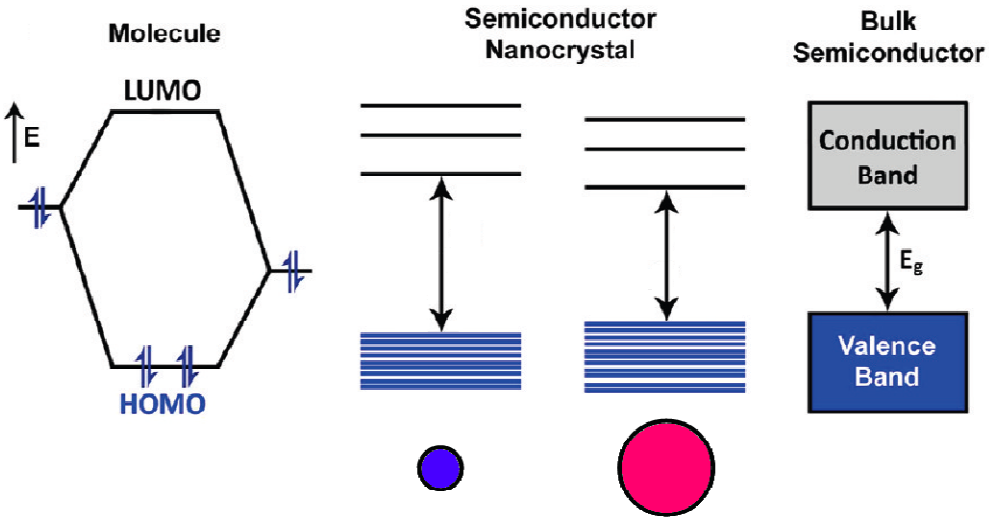

Figure 6: Electronic energy states of a semiconductor in the transition from discrete molecules to nanosized crystals and bulk crystals. Blue shading denotes ground state electron occupation. Adapted with permission from [78] Copyright 2012. American Chemical Society.

When NCs is excited by quanta of energy, an electron is promoted from the valence band into the conduction band, leaving a hole in the valence band (electron-hole pair, i. e. exciton generation). The exciton recombination results in light emission at a wavelength longer than the absorbed light (Stokes shift). Several factors can be used to vary band gap and thus, to control absorption and luminescence wavelengths of the NCs. Classically, band gap engineering can be achieved through the variation of (i) the particle size, or (ii) of the composition. Several alternatives exist for modifying the band gap: (iii) doping the semiconductor host NCs with the incorporation of small amount of impurities, and (iv) modifying the internal structure (homogeneous vs. graded), for example in ternary system QDs like $CdSe_{1-x}Te_x$.[79] Thanks to these strategies, there are now a large variety of QDs that luminesce in the NIR region as illustrated in the figure 7.

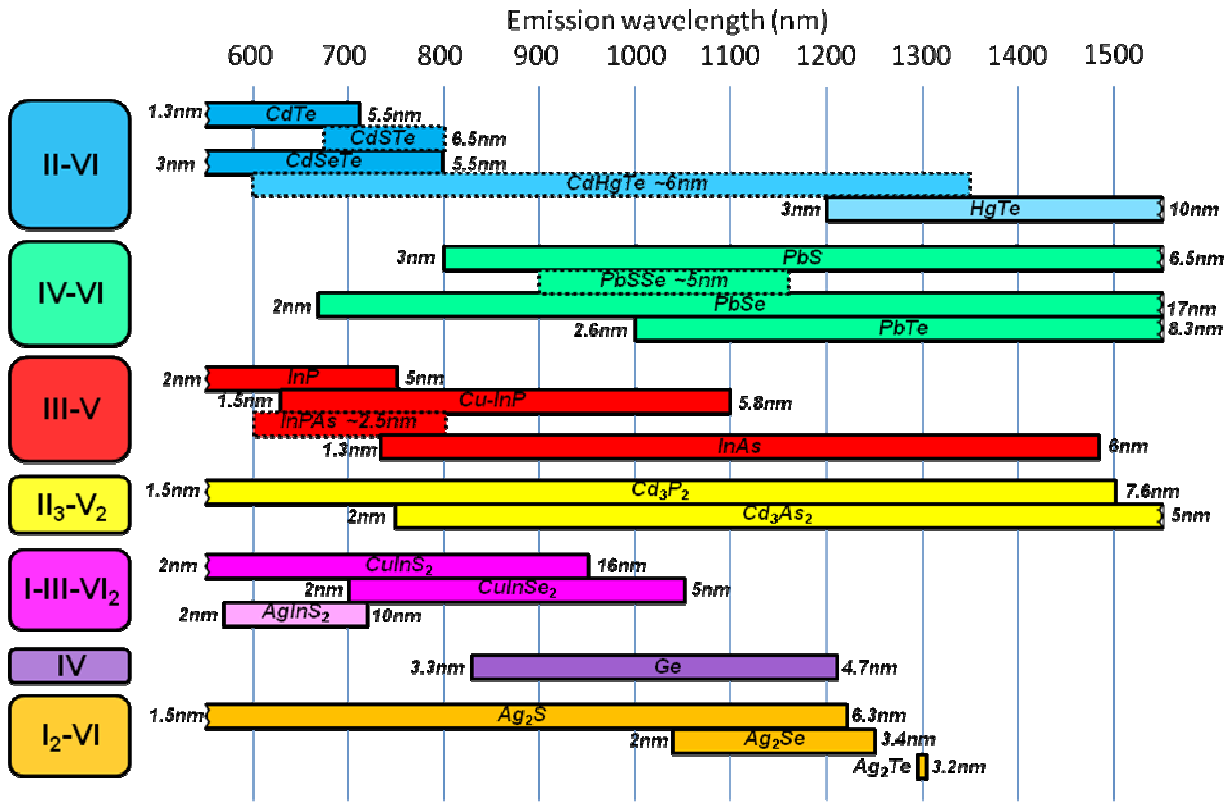

Figure 7: Compositions, sizes and wavelengths ranges of reported NIR-emitting QDs prepared via solution-based methodologies. Emission wavelengths reported for constant size NCs containing different proportions of elements are represented with broken lines rectangle. The references used for the figure are the following: II-VI,[79,80, 81, 82, 83, 84] IV-VI,[85, 86,87, 88, 89] III-V,[90, 91, 92, 93] II_3-V2,[94, 95] I-II-VI2,[96, 97] IV [98,99] and I2-VI [100, 101].

Finally, one can find a last strategy for designing NIR-emitting QDs that is based on core/shell C/S architecture: the core and shell are rationally chosen in order to favor the relaxation of a conduction-band electron of the core into the valence band of the shell (type-II QDs) (Figure 9c).[102] The staggered band alignment leads to a smaller effective band gap than each one of the constituting core and shell materials. This aspect will be described in more details in the “Coating the active core” section devoted to heteronanocrystal, i.e. NCs incorporating two or more materials organized in C/S or core/multishells architecture.

III. 2. Luminescent semiconductor nanocrystals: chemical synthesis of NIR emitting core NCs.

The literature reports a large variety of Cd, Pb or Hg based QDs for which the synthetic routes can be generally classified in two families, according the synthetic medium (aqueous or not). Different protocols have been described in water to produce II-VI semiconductors such as CdTe, $CdSe_xTe_{1-x}$, HgTe, $Cd_xHg_{1-x}Te$, or $Cd_xHg_{1-x}Se$ QDs.[103] The major advantages of this aqueous medium approach are (i) the environmentally friendly medium, (ii) the ease to scale up to gram scale amounts for commercial purpose and (iii) the aqueous compatibility for applications, in particular, biomedical imaging.[104] However, the size distribution is often broad and post-preparative procedures (size-selective precipitation) are required.[80]

In this context, the development of the alternative hot injection method, i.e. the synthesis of NCs in high-temperature boiling organic solvents is considered as one of the main milestones in the chemistry of QDs. The temporal separation of the nucleation and the growth of the seeds gave access to high quality NCs with narrow size distribution (5-10% standard deviation) without laborious size selective precipitation procedure. Since the early works (preparation by Murray et al. of CdE (E = S, Se, Te),[105] synthetic improvements have allowed an ongoing trend toward simpler and safer procedures (replacement of the hazardous [106] or expensive chemicals,[107] decrease of the reaction temperature until ~100 °C [108]). Moreover, the widespread success of the hot-injection strategy is also largely due to its versatility in particular, in terms of chemical variety. The extension of the list of semiconductor materials to high quality (in terms of monodispersity and optical emission) IV-VI QDs such as PbE (E= S,[86] Se, [109] Te [110]), is one of the valuable consequences.[111] Finally, emerging materials such as II_3-V_2 are also worth citing: for

instance, a room temperature procedure has recently be developed to yield Cd_3P_2 QDs which emit in the NIR region [112] and can be envisioned for biodetection. It should also be noted that in case of mercury-based NCs, the aqueous strategy remains the best-suited and almost exclusive approach.[103, 111]

In the context of *in vivo* applications, the issue of metabolic clearance is still an open and unresolved question. To avoid any dilemma, one strategy is to extend the NCs family toward more environmentally friendly elements than Cd, Pb or Hg. [113] We have chosen to detail this attractive perspective in the following paragraphs.

i. Synthesis of Pb-free IV-VI semiconductors NCs (GeE, SnE, E= S, Se, Te).

While the use of precisely-controlled reaction conditions (air- and water-free atmosphere) can be seen as a major drawback when aiming at simple and straightforward procedures, these requirements offer, on the other side, the opportunity to introduce novel precursors yielding to unexplored materials for NCs such as the tin and germanium chalcogenides.[114] The preparation of SnTe NCs [115] using the sophisticated tin complex bis[bis(trimethylsilyl)amino]tin(II) ($Sn[N(SiMe_3)_2]_2$) and trioctylphosphine telluride (TOPTe) was the starting shot toward materials involving these lighter elements of the Pb group. Today, a large variety of compositions (GeS, GeSe, GeTe, $Ge_xSn_{1-x}Se$, SnS_xSe_{1-x}…) and morphology (sphere, sheet, needle) with tunable band gap in the NIR region is accessible.[114] Although the emission properties has not yet been explored, tin and germanium monochalcogenide represent very promising material which would deserve to be tested in the context of biodetection.

ii. Synthesis of III-V semiconductors NCs (InP, InAs).

Following the same tendency toward “greener” material, III-V semiconductors are generally viewed as a highly relevant alternative. This is in particular the case for InP NCs which has been rapidly identified as one of the most promising alternatives to Cd- and Pb-based QDs and has focused the majority of the research efforts devoted to III-V QDs. InP NCs were first prepared in 1994[116] following the, at the time recently published, hot-injection procedure developed for CdE (E = S, Se, Te) QDs with indium oxalate and tris(trimethylsilyl)phosphine ($P(SiMe_3)_3$). Longer reaction times (3-7 days) were required to yield good cristallinity. The progresses towards an easy, reliable and controlled synthesis (*i.e.* in non-coordinating solvent) followed those to their II-VI analogues,[117] but remain one step behind in particular for the size control. The preparation QDs size larger than 5 nm is still a challenging question. This issue is of central importance because, absorption wavelengths higher to 650 nm are at the upper limit of the current attainable range with InP.[90] It has recently been shown that the formation of a mixed oxide shell $InPO_x$ at the surface of the NCs is probably the reason of this growth inhibition. This is the consequence of the oxophilic character of phosphorus and of a side-reaction of the carboxylate ligand occurring at the temperature (230°C-300°C) required for the formation of NCs, which generates oxidative condition in the reaction medium.[118] However, the doping strategy proved to be successful and allow reaching emission wavelength up to 1100 nm.[91] InAs NCs were also prepared following the hot-injection method by typically the reaction of $As(SiMe_3)_3$ and indium chloride [119] or acetate.[117] In the latter case, the QDs size can be controlled to access a range of emission wavelength well-suited for biodetection purpose i.e. between 700 and 1400 nm, with diameters less than ~6 nm.[93]As example, InAs NPs of 3.2 nm of diameter emitting at 750 nm can be easily cleared from the body.[120]

iii. Others semiconductors (IV, I_2-VI and I-III-VI_2 types) for NIR emitting NCs.

Over the last decade, significant progresses have been made concerning the chemistry of NCs of materials alternative to II-VI, IV-VI and III-V. So far, two main families have focused the majority of the research efforts: elemental group IV (Si, Ge) semiconductors and I-III-VI_2 chalcopyrite types like $CuInE_2$ (E = S, Se) or $AgInS_2$. [96] In the latter case, the synthetic strategy is essentially the same than the one developed in the hot injection method for II-VI, IV-VI and III-V materials, i.e. in coordinating (TOPO) [121] or non-coordinating (dioctylphtalate,[122] ODE [123]) solvents. Concerning group IV elements NCs, the synthesis is far less developed. Two main solution strategies exist and involve either strong reducing agents (zintl salts, $LiAlH_4$, K/Na alloy) and/or high-temperature procedures (usually supercritical thermolysis condition).[98] An exception from this rule, is the approaches developed by Boyle's [124] and Klimov's [99] groups who took advantage of the reactivity of Ge(II) precursors using hot injection approach. Very recently, silver chalcogenide Ag2E [101] and in particular silver sulfide Ag_2S [125] were identified as promising materials for NIR-emitting QDs. For these NCs, both aqueous [100, 126, 127] and organic [101, 125, 128] solvents approaches were developed with similar results in terms of size distribution and optical quality, which open the way for *in vivo* studies. [100,126]

IV. Surface modification and probe development

In view of their applications for biological imaging, NPs cannot be use directly after their synthesis for two major reasons. First, because nano-objects have high surface to volume ratios, a large fraction of the constituent atoms are located on the surface. These atoms are incompletely bonded within the crystal lattice, thus disrupting the crystalline periodicity and leaving one or more "dangling orbital" on each atom pointed outward from the crystal. While partially stabilized through dative ligand-metal bonds, the organic passivation is generally

insufficient to provide inertness to the biological medium and/or to air. These surface atoms, indeed, remain highly reactive and are usually prone to oxidation. A general strategy to improve NPs' surface passivation is the overgrowth of a protecting shell around the core, affording chemical stability and preservation of the physical properties. A second requirement aiming at exploiting the magnetic or luminescent properties for biodetection is the solubility of the NPs in physiological media. As discussed in the previous sections, the NPs of best quality are generally produced in non polar solutions using aliphatic coordinating ligand making them insoluble in water. In this context, the phase transfer is an essential but non-trivial step before envisioning their use for biodetection. Finally, the surface of these water-soluble C/S NPs often needs to be engineered for *in-vivo* applications in order to increase the circulation time in the blood stream and enhance their targeting efficiency. The final object is then composed, as depicted in figure 8, of an inorganic core with optimized physical properties, surrounded by an inorganic shell and an organic corona composed of hydrophilic ligands and targeting molecules.

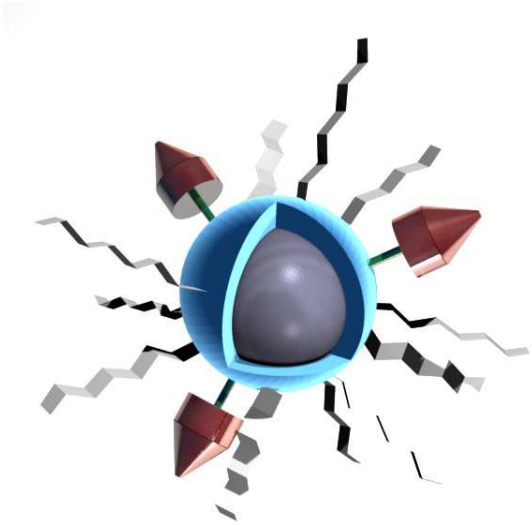

Figure 8. Schematic view of a surface engineered active core (gray) coated with an inorganic shell (blue), hydrophilic surfactants (light gray) and targeting agents (red).

IV.1. Coating the active core

a) Magnetic NPs

Contrarily to iron oxide and ferrite based NPs, metallic NPs which exhibit optimized magnetic properties, are highly reactive towards oxidation. Under air exposure, drastic decrease of the magnetization were reported for Fe [28, 129] and FeCo NPs. [54] Under acidic environment, as encountered by NPs during cell uptake within lysosomes, metallic core disintegrates releasing M^{n+} ions [130] or M• radicals [131] which can lead to the apoptosis of the host cells [130]. Therefore, the outgrowth of a passivating shell is a mandatory step prior to the use of metallic NPs as optimized contrast agents for MRI.

Due to its inertness and its low toxicity, [132] gold would be a perfect candidate for such a protective shell. Though promising results have been reported through transmetallation process [133], the chemical growth of a continuous shell on preformed metallic NPs is challenging, as recently reviewed. [134] Self nucleation of gold yields hybrid objects composed of metallic NPs decorated with small Au islands [135]. Thus, multi-steps physical approach (lithographic process, multiple metal evaporations), though time consuming, have been so far preferred for Co@Au NPs tested for MRI [29]

Oxide shells are alternative candidates which benefits from i) fairly low toxicity levels [136] and ii) simple chemical strategies. The simplest choice relies on the oxide shell which naturally grows at the surface of the metallic core exposed in air. For instance, the native CoO shell is an efficient passivating layer for Co core. In the case of Fe, the stability of Fe@Fe_3O_4 requires a crystalline oxide shell [129]. While such shell is naturally obtained on single crystalline Fe core [28] a controlled oxidation process at high temperature is required for amorphous Fe core [129]. Though CoO and crystalline Fe_3O_4 confer air-stability, these shells

are stable in aqueous media only in a selected pH and ionic strength range. Therefore, SiO_2 coating, due to its remarkable stability in water, has been extensively studied [137]. Silica coating is often grown through water-in-oil microemulsion which may induce an oxidation of the metallic core, thus alternative approaches based on non-alcoholic solvants should be preferred [138, 139]. Additionally, silica shell grown in liquid phase, is generally not fully condensed (incomplete hydrolysis and condensation steps). Thus, post-treatments (annealing as example) are required to make it denser and to prevent a possible permeation to oxygen or any leaching of metallic ions from the core. To the best of our knowledge, such $M@SiO_2$ NPs (M= metal) with a well-condensed shell have never been tested so far neither *in vitro* nor *in vivo*.

Finally, graphitic shell can also be grown to stabilize metallic core either through the calcination of the surrounding ligands [54] or through chemical vapor deposition (CVD) [30]. Such shell has the advantages of being thin, functionalizable and up-to-now, no negative health problems were detected [30]. However, coating of highly reactive Fe NPs should be tested to conclude on the efficiency of such C shell towards oxidation.

b) Quantum dots

In the case of QDs, the role of the shell goes well beyond the sole function of protecting against oxidation and photo-oxidation. The dangling orbitals of the under-coordinated atoms located at the surface may form energy states (“surface energy state”) which quench the luminescence through non-radiative decay paths (Figure 9a).[78] When coating, the dangling bonds are passivated with atoms of the shell, resulting in the dramatic enhancement of the photoluminescence efficiency. As an example, the QY of naked InP NCs is generally inferior to 0.1% but after being coated with ZnS, the QY of the resulting InP/ZnS C/S QDs increases up to 22%.[140] In the majority of cases, the materials chosen for shell are semiconductors

which have a wider band gap than those of core (C/S system called type-I structure) in order to provide electronic insulation thanks to the confinement of both electrons and holes in the core (Figure 9b). A representative (but not exhaustive) list of commonly encountered compositions for NIR emitting C/S NCs is CdTe/MS (M=Zn, Cd), HgTe/CdS, PbSe/PbS, PbSe/CdSe, InP/ZnE (E= S, Se), InAs/InP, InAs/GaAs, InAs/CdSe, Cd_3P_2/ZnS, CuInE/ZnS (E= S, Se).[96, 102, 112] For bio-applications, the shell is generally composed of non toxic elements (e.g. ZnS, prepared with zinc stearate and dodecanethiol) to minimize potential toxic effect by preventing the leaching of element from the core. [102] A general requirement for obtaining highly luminescent C/S QDs is the epitaxial growth of the shell and thus, the use of a material which crystallizes in the same structure than that of the core and has small lattice mismatch with it.[141] The shelling of the QDs is achieved through the slow addition (in order to avoid side-nucleation and formation of separate NCs composed of the shell materials) of the shell precursors into a solution of the purified core. An example of this kind of C/S architecture is $InAs_xP_{1-x}$/InP/ZnSe alloyed QDs for which ZnSe was chosen of its better lattice match to InP than ZnS.[92]

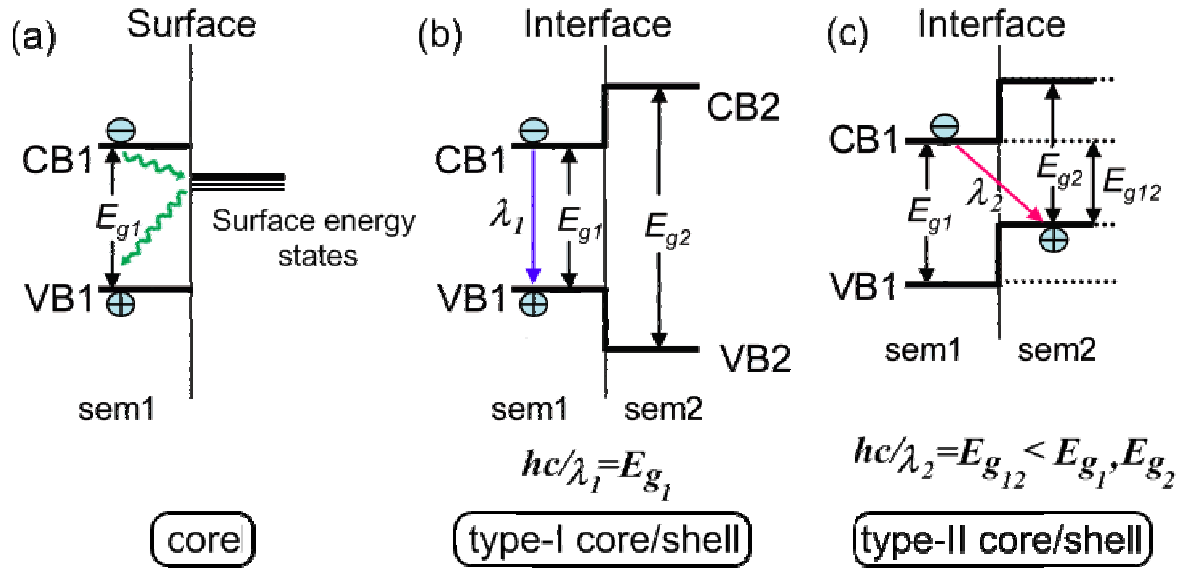

Figure 9. Core a) Type-I, b) and type-II core-shell, c) band-edge alignments at the surface and the heterointerface between two semiconductors. In the type-I structure, both the electron and the hole localize within the material with a narrower energy gap, which is semiconductor 1 (sem1) in the present case. As a result, the wavelength emission, λ_1, is determined by E_{g1}.

The energy gradient existing in the type-II structure tends to spatially separate the electron and the hole on different sides of the heterointerface. In this case, the wavelength emission λ_2 is determined by the energy difference between the conduction band edge of sem1 and the valence band edge of semiconductor 2 (sem2), and hence, it is lower than the band gap of either semiconductor. Adapted with permission from [142] Copyright 2012. American Chemical Society.

Interestingly, by choosing appropriately the shell material, it is possible to tune the emission at wavelengths that cannot be achieved with any of the two materials (those of core and shell) alone. In this type-II system, both the valence and the conduction bands of the shell are lower (or higher) than in the core. As a consequence, this band alignment leads to smaller effective bandgap than each one of the core and the shell material (Figure 9c). This approach is particularly relevant for attaining near-infrared window: for instance, the emission wavelength of the CdTe/CdSe and CdSe/ZnTe C/S heterostructures could be tuned in the NIR range while these emission wavelengths would not be reached by increasing the size of the respective CdTe or CdSe cores.[143] In general, type II C/S QDs have low QY and low photochemical stabilities because one charge (either the electron or the hole) localized in the shell is in direct contact with the surrounding medium and, thus similar reactions than those of naked QDs may occur.[134] These two properties can be improved by coating with another semiconductor material to yield a core multishell structure.[102]

Last, the blinking of QDs which is highly detrimental to their use for single molecule tracking [75] can be suppressed by the coating with thick shells (i.e. 20 monolayers) yielding to a final diameter of ~15 nm.[144] The major drawback is the large size that may be inappropriate for the observation of molecular phenomenon,[75] but this problem have been shown to be possibly circumvented when a composition-graded interface exists between the core and the shell in the more compact (8 nm) CdSe/ZnSe QDs.[145]

IV.2. Phase transfer and surface modification.

a. Phase transfer – water stability - stealth

Phase transfer became an important issue since optimized functional nanoparticles have been prepared in organic solvent, different strategies have been already reviewed [146, 147] and can be sorted, in a first approximation, between two generic approaches (Figure 10):

- ligand exchange : hydrophobic surfactants are replaced by a bifunctional ligand presenting at one end, a function holding a stronger affinity with the NPs surface than the initial ligand and, at the other side, a hydrophilic ending. To enhance the binding affinity and favour a complete replacement of the hydrophobic surfactants, polydendate ligands, such as dimercaptosuccinic acid (DMSA), are often used [24]. This ligand exchange approach is particularly useful to stabilize water-soluble nanoparticles with small hydrodynamic size (<20nm), but may lead to particle aggregation and loss of optical properties for QDs [147]. This problem is commonly encountered for C/S QDs such as CdSe/ZnS,[148] InP/ZnS [149] or the other NIR-emitting material $CuInS_2$/ZnS.[150] Recently, Reiss et al. have given insight on the precise mechanism, attributing the quenching to hole transfer from the QDs to the capping ligand (cysteine) resulting in the formation of the cysteine dimer (cystine).[150]

- copolymer addition : amphiphilic surfactants are added, their hydrophobic tails form weak interactions with the existing hydrophobic coating while their hydrophilic groups are exposed, ensuring the water-solubility. Variety of lipophilic polyethylene glycol (PEG)-based polymers have been used [147] Such copolymer strategy leads to a drastic increase of the hydrodynamic size of the NPs (>20nm) but ensures a fairly long blood circulation due to PEG moities [151].

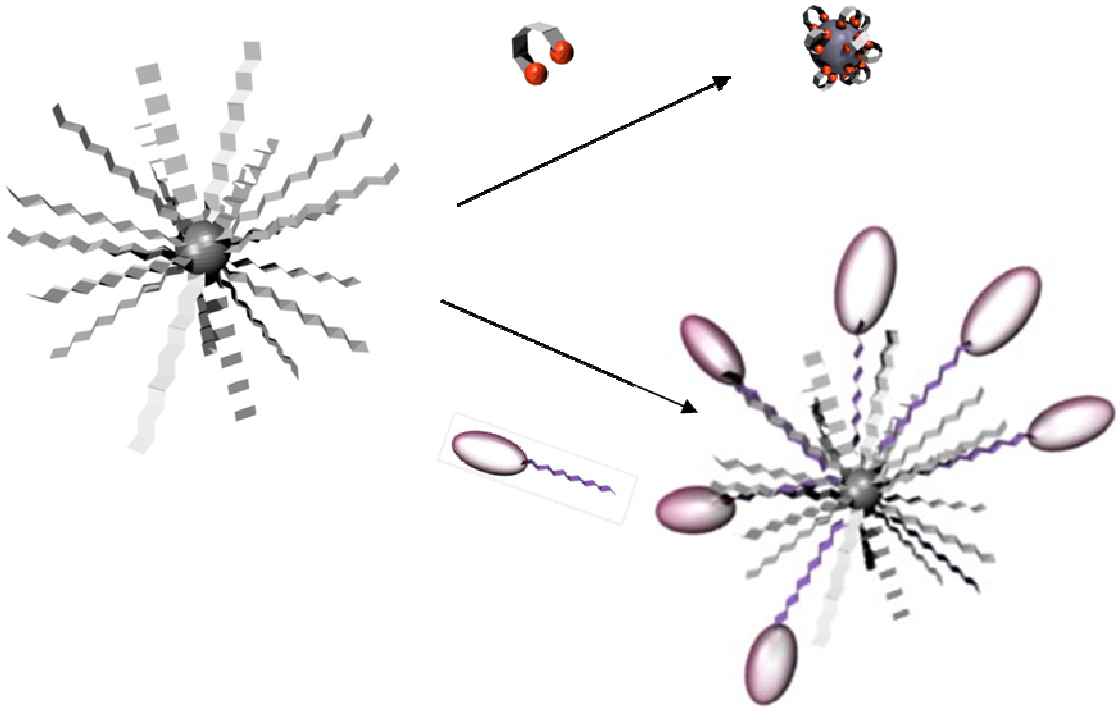

Figure 10. Schematic view of the three generic strategies for water transfer of hydrophobic NPs : through ligand exchange or copolymer addition.

The choice of the functionalization strategy results from a delicate balance between the surface state chemistry of the NPs and the final hydrodynamic diameter reached. Hydrodynamic size influences the relaxativity constant and drives the interactions with tissues and biological media (through size dependent diffusion). While ultra-small particles (ca. 5nm) are quickly excreted by the kidney, intermediate NPs (15-100 nm) exhibit longer circulation time [152],larger NPs (> 100 nm) being more susceptible to opsonisation (uptake by the immune defence system). Thus, the functionalization strategy must be carefully chosen in order to reach the optimized window of hydrodynamic size (15-100nm).

In addition to the hydrodynamic size effect, the pharmacokinetics and biodistribution of nanoparticles is driven by surface coating. Lifetime in blood circulation strongly depends on the interaction of the NPs with plasma proteins (opsonins). Accumulations of opsonins are

recognized by reticuloendothelial system (RES) and phagocyted by macrophages Grafting of PEG on the surface of NPs may inhibit the protein interaction and prolong the blood circulation time. [153] This effect strongly depends on the conformation of the PEG chains at the NPs surface, which evolves from mushroom to brush configurations for longer PEG chain (≥ 2000 Da) and higher surface density. [153] While brush configurations generate greater protein repulsion, it may also lower the nanoparticle targeting efficiency due to the sterically shielding of the specific agents. [154] Therefore, targeting agents should be conjugated to PEG-spacer of similar length to stand at the outmost exterior of the NPs, lying above the organic corona. [153]

b. Cancer cell targeting

Numerous reports have shown that most NPs accumulate in tumors due to enhanced permeation and retention (EPR) effect, which results from relatively large and permeable blood vessels along with poor lymphatic drainage of tumor cells. [153] For instance, iron oxide NPs were successfully used to diagnose cancer without any targeting agents [155]. Such cancer cell uptake strategy is referred to as passive targeting and let consider a possibility of universal labeling. Charged NPs have been tested in the seeking of universal labeling but controversial results have been found. While anionic NPs (citrate) have been reported as exhibiting a better cell-uptake than cationic or uncharged NPs, [156] another study shows that cationic (aminodextran) NPs were optimized. [157] Though contradictory, these results might

be explained by the tendency of charged NPs to be destabilized under harsh pH and ionic strength environment, as encountered in biological media.

In order to enhance the selective internalization of NPs, active targeting strategies were developed. Driven at the vicinity of tumor cells by EPR effect, NP grafted with adequate moieties would be internalized faster through receptor-mediated endocytosis. Such tumor surrounding clearance generates a diffusion gradient which can favor the further NP flow, and thus, the accumulation of NP within the tumor region. [153] One of the main challenges of active targeting is the design of adequate targeting moieties. Indeed, tumor cells exhibit receptors fairly similar to the surrounding healthy cells, the difference being their relative abundance. Therefore, targeting agent must specifically bind to overexpressed receptors. Small molecules, peptides, proteins, aptamers and antibodies have demonstrated high affinity with receptors overexpressed in malignant cells as previously reviewed.[2, 22, 153]. A key issue during the grafting of such moieties onto the NP surface is to maintain their affinity for receptors. Their density, accessibility and conformation should be preserved, thus, spacers are often added to avoid shielding and denaturing of the ligand.

V. Applications

In this part, we aim to illustrate the recent progress in MRI and NIR *in vivo* real time imaging due to the use of new generation of magnetic nanoparticles and QDs. A last part will aim at presenting the recent very first tries of combination of both properties in multimodal single nano-objects and the promises of this strategy.

V.1 MRI in vivo

In this part, we aim to illustrate the recent progress in *in vivo* MRI due to the use of new generation of magnetic nanoparticles. The main objective is to evaluate the potentialities of the latter to favour further developments in this field of application. Reviews on MRI using "classical" MNPs (SPIO, USPIO) can be referred to for comparison purpose; they generally describe *in vivo* MRI experiments dealing with cancer, cardiovascular disease or molecular imaging.[158] Here, we only report examples of MRI improvements due to new contrast agents. Moreover, we like to mention studies that directly compare MNPs whose magnetic materials were of different nature, but coating and functionalization were identical. This way, the other parameters that necessarily impact the MRI response (coating thickness, bio-distribution…) can be considered unchanged.

As previously explained, the main reason to work on magnetic composition of contrast agents, is to enhance the contrast on MR images. In a recent study reported by Cheong *et al.*, it was shown that Fe/FeOx core/shell NPs improve by a factor 2 the contrast in T2-weighted MR images of mice nodes compared to pure FeOx NPs. Interestingly, they allow for a much better *in vivo* detection of small tumors (1-3 mm) at 1.5 T. [27] *In vivo* probing of small-sized cancers (~50 mg) with manganese ferrites NPs coated with DMSA and conjugated with the cancer-targeting antibody Herceptin was successful too as reported by the Cheon's group. [24]. On the contrary, the analogue pure iron oxide nanoparticles did not allow such performances. The authors attribute this promising result to the higher saturation magnetization of the manganese ferrites nanoparticles. Developed by Chen *et al.*, the 12 nm-FePt nanoparticles conjugated to the anti-Her2 monoclonal antibody showed significant contrast enhancement in both MRI and computated tomography (CT), thus taking advantage of their magnetic properties and the high X-ray absorption of platinum. [159] Indeed, 24h after injection (28 mM Fe concentration, 100 μL) into mice bearing transplanted MBT2 tumor,

the MR images showed 51% intensity reduction on the tumor lesion while CT image analysis revealed 138% contrast enhancement. In addition, the biodistribution of the non-fonctionalized FePt nanoparticles evaluated on mice suggest that they could be cleared from the body after about 1 week.

The FeCo@graphitic carbon (GC) nanocrystals prepared by Dai *et al.* showed unusually higher r1 and r2 values than conventional Gd and iron-oxide-based contrast agents [30]. As an example, they allowed for positive contrast enhancement on T1-weighted MR images of the blood pool in the rabbit (see Figure 11).

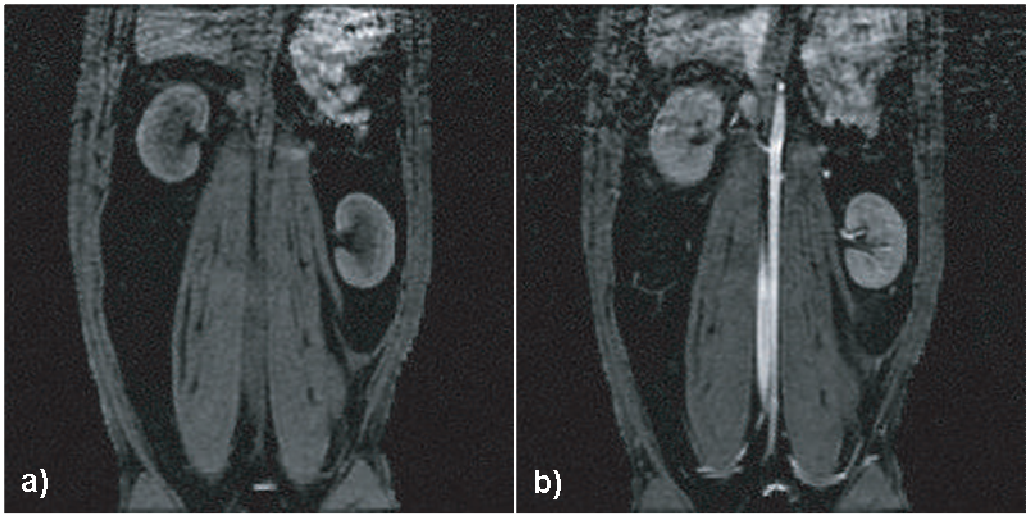

Figure 11. T1-weighted MR images of a rabbit a) before and b) 30 min after initial Injection of a solution of 4nm FeCo/GC nanocrystals (metal dose 9.6 µmol.kg-1 for the 5kg rabbit). The blood pool in the aorta is significantly brightened (positive contrast) in the MRI after injection. We also see signal increase in the kidney medulla and cortex due to the high blood volume within the kidney. We see little signal enhancement in the muscle. Reprinted with permission from Macmillan Publishers Ltd : Nature Materials [30].Copyright 2006.

This was 30min after NPs injection using a metal dose of only 10% of what was typically used for existing Gd agents (metal dose ~9.6 µmol kg−1 for the ~5 kg rabbit). The authors claim that this represents an important achievement in MRI contrast-agent development; long-circulating positive-contrast enhancement at low metal dosages *in vivo* is indeed particularly interesting for angiographic MR images.

The Co@Au nanowontons reported by Bouchard *et al.* were dual-modality MRI/photoacoustic tomography (PAT) contrast agent.[29] Even when injected in mice muscle leg at concentration as low as 50 pM, a negative contrast was clearly detected on T_2-weighted spin echo MR images (see Figure 12). Interestingly, this degree of sensitivity is approaching the one of radioactive labels. PAT detection was also conclusive as observe for a rat tail local injection of 100 pM of nanowontons.

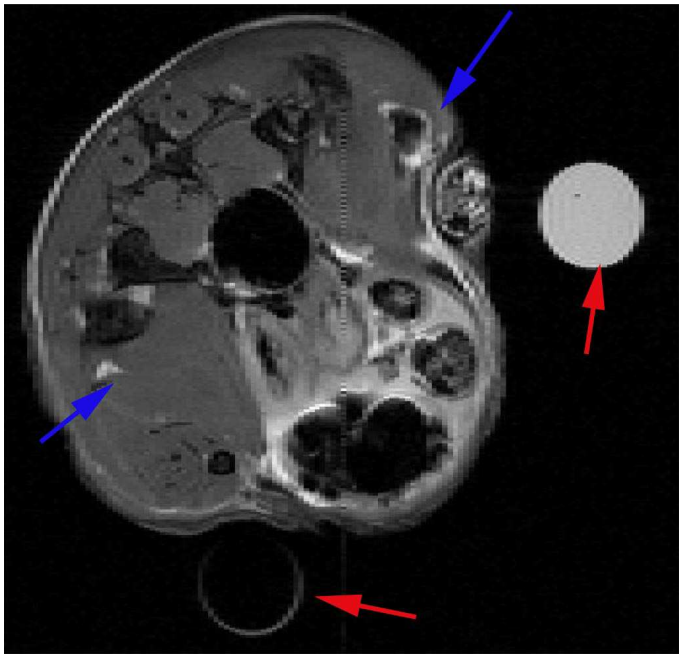

Figure 12. Transverse (axial) MRI image in mouse leg muscle injected with Co nanowontons in PBS solution. The position of the blue arrows indicates the sites of injection for the nanowontons (upper right corner) and the PBS control (lower left corner). Two water-carrying test tubes are also visible in the scans for purposes of MRI slice alignment (red arrows). MRI parameters were: TE = 50 ms; TR = 1 s; field of view is 2.6 cm × 2.6 cm, and slice thickness is 0.5 mm.

V.2 Luminescence

Thanks to their remarkable features, NIR emitting QDs have become one of the mainstays of *in vivo* imaging modalities.[160] This success story started a decade ago with the real-time mapping of sentinel lymph nodes in mouse and pig, using type II C/S CdTe/CdSe QDs.[161] Since this significant achievement, progresses have been made in several main domains:

biodistribution of QDs, tumors imaging, tracking of cells and vascular imaging (blood vessel and lymphatic circulatory system).[104, 160]

Unfortunately, these results have been obtained using toxic elements such as Cd, Pb, Hg, or As. The toxicity concerns associated to this family of materials have fueled researches for their replacement with non-toxic elements. The relevancy of these materials ($CuInE_2$/ZnS, [97, 162, 163, 164, 165] InP/ZnS, [166]' Ag_2E [100, 126] with E= S, Se) for in vivo NIR imaging have been proven in the very recent years in the context of biodistribution,[163] tumor [162, 166]and lymph imaging.[97, 164] The lower *in vivo* toxicity of these alternative material QDs has been examined and experimentally confirmed for $CuInS_2$/ZnS and InP/ZnS.[164, 166]

As a representative example of the potential of such a tool for realtime in vivo visualization, Reiss et al. monitored the fluorescence distribution of $CuInS_2$/ZnS QDs (functionalized with dihydrolipoic acid yielding a hydrodynamic diameter of ~17 nm) with time (Figure13). [163] QDs were injected intravenously into the tail of nude mouse and after 15 min, they accumulate essentially in the liver, spleen and lungs (fluorescence in the stomach is attributed to the feed).

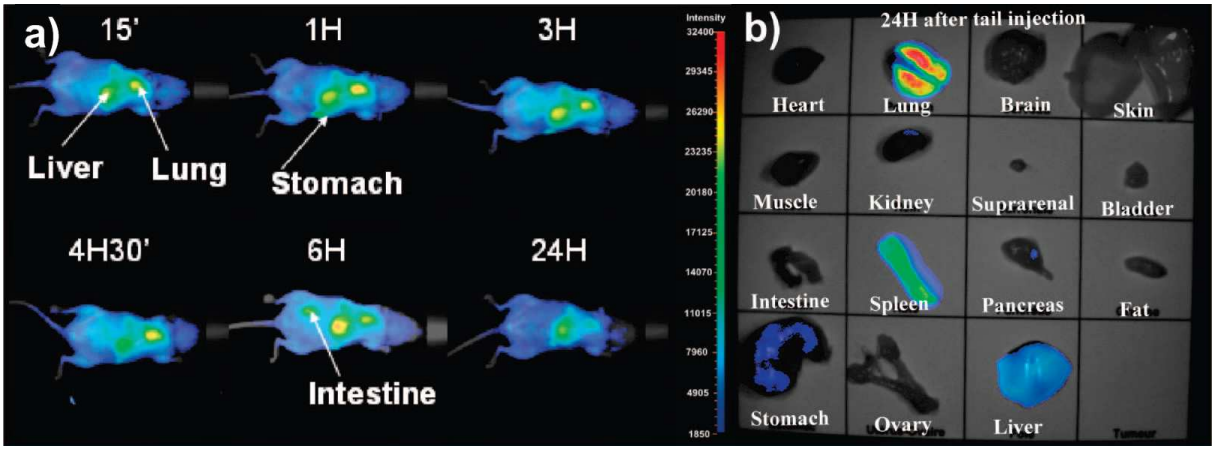

Figure 13. a) Fluorescence images (excitation wavelength 633 nm) showing the temporal evolution of the biodistribution of the $CuInS_2$/ZnS NCs injected intravenously into the tail of a healthy nude mouse (eq 6.5 × 1016 to 1.3 × 1017 copper atoms). The integration time is 200 ms and the contrast has been set between 1850 and 32400. b) Fluorescence images of the different parts of the mouse after dissection. Adapted with permission from [163] Copyright 2012. American Chemical Society.

Additionally, Gu et al. recently demonstrated for the first time the capability for in vivo multiplex imaging, using two different NIR-emitting QDs.[162] 720 nm and 800 nm emitting $CuInS_2$/ZnS NCs were injected into the mouse subcutaneously respectively in the right and left paw (Figure 14).

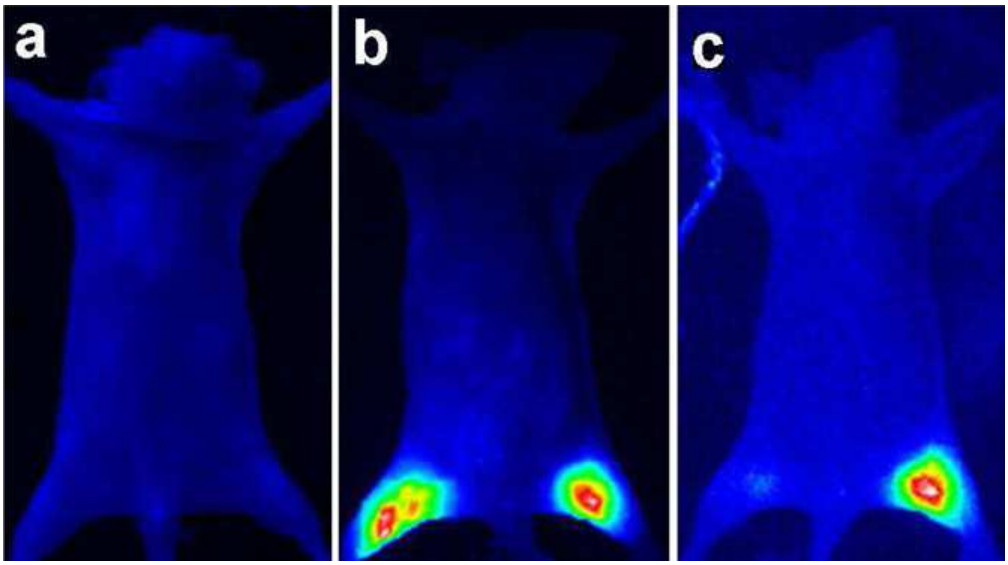

Figure 14. Multiplex NIR fluorescence imaging of mouse administered with two different NIR-emitting QDs-loaded micelles by subcutaneous injection (the right leg, 720 nm-emitting NCs; the left leg, 800 nm emitting NCs): (a) before injection, (b) λ_{ex} = 660 nm, a 700 nm long pass filter, (c) λ_{ex} = 766 nm, an 800 nm long pass filter. Adapted with permission from [162] Copyright 2012. American Chemical Society.

When excited at 660 nm, both types of QDs can be observed while only the fluorescence signal of the left leg remained very bright when irradiation occurs at 766 nm. This result indicates that $CuInS_2$/ZnS QDs could be use for in vivo multiplexed imaging of molecular by selecting the appropriate excitation wavelength or filter (not shown here).[162]

However, the progress differs significantly according to the materials: while being highly promising, the Ag_2E-based QDs (E= S, Se) are still, in the first stage of development with the proof of principle of *in vivo* NIR fluorescence penetrability.[100, 126] In contrast, impressive results were recently reported by Cheng et al. with sophisticated biocompatible Dendron-coated InP/ZnS QDs (hydrodynamic diameter ~12 nm).[166] These latter satisfy many of the

requirements (near-infrared emission with high efficiency, high stability in biological media, biocompatibility, suitable small size with possible renal clearance, ability of extravasation) for clinical translation. In the corresponding article, they were used as nanoprobes to demonstrate *in vivo* the highly specific targeting of Dendron-RGD_2 for imaging integrin αvβ3-positive tumors. The fluorescent signals derived from InP/ZnS NCs functionalized respectively with Dendron and Dendron-RGD_2 were monitored in real time over 28h (Figure 15). Thanks to the high sensivity of these QDs, the difference of behavior induced by the different functionalization could be evidenced. In the case of Dendron-RGD_2 functionalization, the long-term retention is clearly observed from the fluorescence signal at the tumor site (indicated by the arrow, Figure) which carries on after 28h. On the contrary, the tumor uptake of InP/ZnS QDs-Dendron with visible contrast from surrounding tissues can be observed between 4 and 6 hours and then disappears. This behavior was assigned to enhanced permeability and retention (EPR) effect for the suitably small-sized InP/ZnS QDs-Dendron.

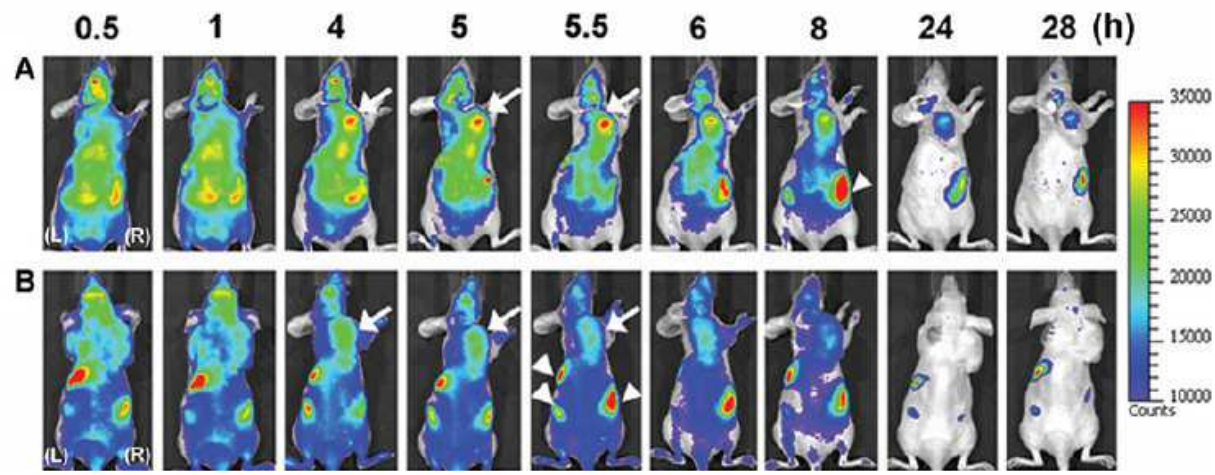

Figure 15. The dorsal images of SKOV3 tumor-bearing (arrows) mice injected with (A) InP/ZnS-Dendron-RGD2 (200 pmol) and (B) InP/ZnS-Dendron (200 pmol) at 0.5, 1, 4, 5, 5.5, 6, 8, 24, and 28h, respectively. The incidental high fluorescent signals in other body parts (arrowheads) might have originated from regular rodent food in stomach and feces in intestine. Reprinted with permission from [166] Copyright 2012. American Chemical Society.

V.3 Multimodal

Recently, hybrid NPs combining at least two properties have received lots of interest as shown by the increasing number of dedicated reviews [167, 168]. Combining optic and magnetic properties within the same nano-object would open new perspectives towards multimodal imaging (NIR, MRI), [169] and theranostic applications, coupling detection and treatment potentialities. [170] However, one of the main issues is to keep both physical properties unaltered. QD luminescence can be strongly reduced due to electron transfer and competitive light absorption with the magnetic material. The direct growth of QD onto magnetic NPs, forming FePt-QDs heterodimers [171] or FePt@CdSe core/shell structure, [172] results in an prominent quenching of the fluorescence. [173] Analogously, the growth of Co tips onto preformed CdSe nanorods results in a emission intensity 30 times lower than that of pure CdSe rods. [174]

To prevent the electron transfer which results in the luminescence quenching, QD and magnetic material could be isolated. One strategy is based on the use of metal oxide, insulating material, as the magnetic component of the heterodimer. Gao et al. have shown that Fe_3O_4-CdSe NPs exhibit quantum yield as high as 38%,[175]. Such fluorescence enables the intracellular detection of the NPs, however no results were reported regarding their magnetic properties nor their relaxativity. In order to favour metallic materials which exhibit higher magnetization, a solution consists in incorporating preformed magnetic NPs and QDs into an isolating matrix (such as silica). [176] However, the resulting object exhibits a high hydrodynamic volume, which may be a drawback for further in-vivo applications and prevents the diffusion of water proton at the vicinity of the magnetic NPs, resulting in poor relaxativity. [177] Deka et al. have reported a promising approach based on the intercalation of a semiconductor with larger band gap between the metallic part and the QD, which may result in decoupling QD and metal electronic states. [178] CdSe@CdS decorated with Co tips

exhibited preserved magnetic properties (M_S=148 emu/g_{Co}) but partially quenched fluorescence (QY = 3%). Optimization of the spacer nature and thickness could be pursued to retain both physical properties unaltered.

Conclusion :

In this review paper, we have presented the potentiality of a new generation of optimized contrast agents, based on metallic NPs and Hg, Cd, Pb, As free QDs, for respectively MRI and NIR imaging. Though extensive literatures can be found on well established iron oxide NPs or Cd-based quantum dots, only few reports outline the requirements that new probe generation should fulfil. Thanks to the description of the physics of the imaging techniques, optimized materials could be enlightened as long as the syntheses which yield to the corresponding NPs. Surface engineering strategies to ensure the biodistribution and the specific targeting of inorganic NPs were reviewed. The resulting NPs combines, through a complex architecture, the optimized inorganic core surrounded by a non-porous coating shell, to ensure the stability of the core, an organic corona to reach adequate biodistribution and targeting moities to enhance the specific cellular uptake. Few results demonstrate the *in vivo* potentiality of these new generations of probes. Drastic enhancement of relaxativity (up to 10^5 times) was observed for Co based NPs, while impressive fluorescent results were obtained for Cd-free InP/ZnS QDs. The next step towards the optimization of contrast agents relies on the integration, within a single object, of MRI and NIR imaging potentialities. Such multimodal NPs, though extremely promising, requires the strict decoupling of semiconducting and metallic electronic states. The introduction of a large gap semiconductor spacer could be the most promising approach which could yield to unaltered magnetic and optic properties.

[1] Cassidy, P. J. ; Radda, G. K. 2005 Molecular imaging perspectives, *J. R. Soc. Interface* , 2, 133–144 (DOI:10.1098/rsif.2005.0040)

[2] Cho, E. C. ; Glauss, C. ; Chen, J. ; Welch, M. J.; Xia, Y. 2010, Inorganic nanoparticle-based contrast agents for moleuclar imaging, *Trends Mol. Med.*, 16 (12), 561-573 (DOI:10.1016/j.molmed.2010.09.004)

[3] Lee, D.-E.; Koo, H.; Sun, I.-C.; Ryu, J. H.; Kim, K.; Kwon, I. C. 2012 Multifunctional nanoparticles for multimodal imaging and theragnosis, *Chem. Soc. Rev.*, 41, 2656–2672 (DOI: 10.1039/c2cs15261d).

[4] Hötzer, B.; Medintz, I. L.; Hildebrandt N. 2012 Fluorescence in Nanobiotechnology: Sophisticated Fluorophores for Novel Applications, *Small*, 8, 2297–2326 (DOI: 10.1002/smll.201200109).

[5] Lacroix, L.-M.; Ho, D.; Sun, S. 2010. Recent advances in Magnetic Nanoparticles for Diagnostic and Therapeutic Applications, *Curr. Top. Med. Chem.*, 10, 1184 – 1197

[6] Finney, E. E.; Finke, R. G. 2008 Nanocluster nucleation and growth kinetic and mechanistic studies: A review emphasizing transitionmetal nanoclusters. *J. Colloid Interface Sci.*, 317, 351-374 (DOI: 10.1016/j.jcis.2007.05.092)

[7] LaMer, V. K.; Dinegra, R. H. 1950 Theory, production and mechanism of formation of monodispersed hydrosols. *J. Am. Chem. Soc.*, 72, 4847-4854 (DOI: 10.1021/ja01167a001)

[8] Park, J.; Joo, J.; Kwon, S. G.; Jang, Y.; Hyeon, T. 2007. Synthesis of monodisperse spherical nanocrystals, *Angew. Chem. Int. Ed.* 46, 4630-4660 (DOI: 10.1002/anie.200603148)

[9] Shevchenko E. V.; Talapin, D. T.; Schnablegger H.; Kornowski, A.; Festin O.; Svedlinh, P.; Haase, M.; Weller, H. 2002. Study of nucleation and growth in the organometallic synthesis of magnetic alloy nanocrystals : the role of nucleation rate in size control of $CoPt_3$ nanocrystals, *J. Am. Chem. Soc.* 125, 9090-9101 (DOI : 10.1021/ja029937l)

[10] Lin, W. ; Hyeon, T. ; Lanza, G. M. ; Zhang, M. ; Maede, T. J. 2009. Magnetic nanoparticles for early detection of cancer by magnetic resonance imaging. *MRS Bull.* 34, 441-448 (DOI: 10.1557/mrs2009.120)

[11] Caravan, P. ; Ellison, J. L.; McMurry, T. J. ; Lauffer, R. B. 1999. Gadolinium(III) chelates as MRI contrast agents : structure, dynamics and applications. *Chem. Rev.* 99, 2293-2352 (DOI : 10.1021/cr980440x)

[12] Caravan, P. 2006. Strategies for increasing the sensitivity of gadolinium based MRI contrast agents. *Chem. Soc. Rev.* 35, 512–523 (DOI: 10.1039/B510982P)

[13] De Leon-Rodriguez, L. M.; Lubag, A. J. M.; Malloy, C. R.; Martinez, G. V.; Gillies, R. J.; Sherry, A. D. 2011 Responsive MRI agents for sensing metabolism in vivo. *Acc. Chem. Res.* 42, 948-957 (DOI : 10.1021/ar800237f)

[14] Na, H. B.; Song, I. C.; Hyeon, T. 2009. Inorganic nanoparticles for MRI contrast agents. *Adv. Mater.* 21, 2133-2148 (DOI : 10.1002/adma.200802366)

[15] Cheon, J. ; Lee, J.-H. 2008. Synergistically integrated nanoparticles as multimodal probes for nanobiotechnology, *Acc. Chem. Res.* 41 (12), 1630-1640 (DOI : 10.1021/ar800045c)

[16] Tromsdorf, U. I. ; Bigall, N. C.; Kaul, M. G.; Bruns, O. T.; Nikolic, M. S.; Mollwitz, B.; Sperling, R. A.; Reimer, R.; Hohenberg, H.; Parak, W. J.; Forster, S.; Beisiegel, U.; Adam, G.; Weller, H. 2007. Size and surface effects on the MRI relaxativity of manganese ferrite nanoparticle contrast agents, *Nano Lett.* 7, 2422-2427 (DOI : 10.1021/nl071099b)

[17] Lee, N. ; Choi, Y. ; Lee, Y. ; Park, M. ; Moon, W. K.; Choi, S. H.; Hyeon, T. 2012. Water-dispersible ferromagnetic iron oxide nanocubes with extremely high r2 relaxativity for highly sensitive in vivo MRI of tumors. *Nano Lett.* 12, 3127-3131 (DOI : 10.1021/nl3010308)

[18] Lee, J. S.; Tan, R. P.; Wu, J. H.; Kim, Y. K. 2011. Effect of interparticle interactions and size dispersión in magnetic nanoparticle assemblies : a static and dynamic study. *Appl. Phys. Lett.* 99, 062506 (DOI : 10.1063/1.3624833)

[19] Yang, Y.; Liu, X.-L.; Yi, J.-B.; Yang, Y.; Fan, H.-M.; Ding, J. 2012 Stable vortex magnetite nanorings colloid: micromagnetic simulation and experimental demonstration. *J. Appl. Phys.* 111, 044303 (DOI : 10.1063/1.3684963)

[20] Snoeck, E. ; Gatel, C. ; Lacroix, L.-M. ; Blon, T. ; Lachaize, S. ; Carrey, J. ; Respaud, M. ; Chaudret, B. 2008. Magnetic configurations of 30nm Iron Nanocubes Studied by Electron Holography *Nano Lett.*, 8, 4293-4298 (DOI : 10.1021/nl801998x)

[21] Lacroix, L.-M.; Lachaize, S.; Hue, F. ; Gatel, C. ; Blon, T. ; Tan, R. P. ; Carrey, J. ; Warot-Fonrose, B. ; Chaudret B. 2012, Stabilization vortices in interacting nano-objects : a chemical approach. *Nano Lett.* 12, 3245-3250 (DOI : 10.1021/nl3012616)

[22] Yang, F. ; Jin, C. ; Subedi, S. ; Lee, C. L.; Wang, Q.; Jiang, Y.; Li, J.; Di, Y.; Fu, D. 2012 Emerging inorganic nanomaterials for pancreatic cancer diagnosis and treatment. *Cancer Treat. Rev.* 38, 566-579 (DOI : 10.1016/j.ctrv.2012.02.003)

[23] Huang, S.-H. ; Juang, R.-S. 2011. Biochemical and biomedical applications of multifunctional magnetic nanoparticles : a review. *J. Nanopart. Res.* 13, 4411-4430 (DOI : 10.1007/s11051-011-0551-4)

[24] Lee J.-H. ; Huh, Y.-M. ; Jun, Y.-W. ; Seo, J.-W. ; Jang, J.-T. ; Song, H.-T.; Kim S.; Cho, E.-J.; Yoon, H.-G.; Suh, J. S.; Cheon, J. 2007 Artificially engineered magnetic nanoparticles for ultra-sensitive molecular imaging, *Nature Med.* 13, 95-99 (DOI : 10.1038/nm1467)

[25] Duan, H.; Kuang, M.; Wang, X.; Wang, Y. A.; Mao, H.; Nie, S. 2008. Reexamining the effects of particle size and surface chemistry on the magnetic properties of iron oxide nanocrystals : new insights into spin disorder and proton relaxivity, *J. Phys. Chem. C*, 112, 8127-8131 (DOI: 10.1021/jp8029083)

[26] Hadjipanayis, C. G.; Bonder, M. J.; Balakrishnan, S.; Wang, X.; Mao, H.; Hadjipanayis, G. C. 2008. Metallic Iron Nanoparticles for MRI Contrast Enhancement and Local Hyperthermia, *Small*, 4, 1925-1929 (DOI : 10.1002/smll.200800261)

[27] Cheong, S. Ferguson, P. ; Feindel, K. W.; Hermans, I. F.; Callaghan, P. T.; Meyer, C.; Slocombe, A.; Su, C.-H.; Cheng, F.-Y.; Yeh, C.-S.; Ingham, B.; Toney, M. F.; Tilley, R. D. 2011. Simple synthesis and functionalization of iron nanoparticles for magnetic resonance imaging. *Angew. Chem. Int. Ed.* 50, 4206-4209 (DOI : 10.1002/anie.201100562)

[28] Lacroix, L.-M. ; Huls, N. F. ; Ho, D. ; Sun, X. ; Cheng, K.; Sun, S. 2011. Stable single-crystalline body centered cubic Fe nanoparticles, *NanoLett.* 11, 1641-1645 (DOI : 10.1021/nl200110t)

[29] Bouchard, L.-S. ; Anwar, M. S. ; Liu, G. L. ; Hann, B. ; Xie, Z. H. ; Gray, J. W. ; Wang, X.; Pines, A.; Chen, F. F. 2009 Picomolar sensitivity MRI and photoacoustic imaging of cobalt nanoparticles. *Proc Nat. Am. Soc.* 106, 4085-4089 (DOI : 10.1073/pnas.0813019106)

[30] Seo, W. S.; Lee, J. H.; Sun, X.; Suzuki, Y.; Mann, D.; Liu, Z.; Terashima, M.; Yang, P. C.; McConnell, M. V.; Nishimura, D. G.; Dai, H. 2006 FeCo/graphitic-shell nanocrystals as advanced magnetic-resonance-imaging and near-infrared agents. *Nat. Mater.* 5, 971 – 976 (DOI : 10.1038/nmat1775)

[31] Maesono S. ; Suzuki, T. ; Saita, S. 2008 Superparamagnetic FePt nanoparticles as excellent MRI contrast agents. *J. Magn. Magn. Mater.* 320, L79-L83 (DOI : 10.1016/j.jmmm.2008.01.026)

[32] Huang, S.; Yan, W.; Hu, G.; Wang, L. 2012. Facile and green synthesis of biocompatible and bioconjugatable magnetite nanofluids for high-resolution T2 MRI contrast agents. *J. Phys. Chem. C.* 116, 20558-20563 (DOI : 10.1021/jp305211d)

[33] Laurent, S.; Forge, D.; Port, M.; Roch, A.; Robic, C.; Vander Elst, L.; Muller, R. N. 2008 Magnetic iron oxide nanoparticles: synthesis, stabilization, vectorization, physicochemical characterizations, and biological applications. *Chem. Rev.*, 108, 2064-2110 (DOI: 10.1021/cr068445e)

[34] Park, J.; Lee, E.; Hwang, N.-M.; Kang, M.; Kim, S. C.; Hwang, Y.; Park, J.-G.; Noh, H.-J.; Kim, J.-Y.; Park, J.-H.; Hyeon T. 2005. One-Nanometer-Scale Size-Controlled Synthesis of Monodisperse Magnetic Iron Oxide Nanoparticles. *Angew. Chem. Int. Ed.* 44, 2872-2877 (DOI : 10.1002/anie.200461665)

[35] Sun, S.; Zeng, H. 2002 Size-controlled synthesis of magnetite nanoparticles. *J. Am. Chem. Soc.* 124, 8204-8205 (DOI : 10.1021/ja026501x)

[36] Reddy, L. H.; Arias, J. L.; Nicolas, J.; Couvreur, P. 2012. Magnetic nanoparticles : design and characterization, toxicity and biocompatibility, pharmaceutical and biomedical applications. *Chem. Rev.*, 112, 5818-5878 (DOI : 10.1021/cr300068p)

[37] Lee, N.; Hyeon, T. 2012. Designed synthesis of uniformly sized iron oxide nanoparticles for efficient magnetic resonance imaging contrast agents. *Chem. Soc. Rev.*, 41, 2575-2589 (DOI : 10.1039/C1CS15248C)

[38] Sun, S.; Zeng, H.; Robinson, D. B.; Raoux, S.; Rice, P. M.; Wang, S. X.; Li, G. 2004. Monodisperse MFe2O4 (M= Fe, Co, Mn) nanoparticles. *J. Am. Chem. Soc.* 126, 273-279 (DOI : 10.1021/ja0380852)

[39] Huber, D. 2005 Synthesis, properties, and applications of iron nanoparticles. *Small*, 1, 482-501 (DOI: 10.1002/smll.200500006)

[40] Yang, H.; Ito, F.; Hasegawa, D.; Ogawa, T.; Takahashi, M. 2007 Facile large-scale synthesis of monodisperse Fe nanoparticles by modest-temperature decomposition of iron carbonyl, *J. Appl. Phys.*, 101, 09J112 (DOI: 10.1063/1.2711391)

[41] Farrell, D.; Majetich, S. A.; Wilcoxon, J. P. 2003 Preparation and Characterization of Monodisperse Fe Nanoparticles, *J. Phys. Chem. B*, 107, 11022-11030 (DOI : 10.1021/jp0351831)

[42] Meffre, A.; Mehdaoui, B.; Kelsen, V.; Fazzini, P. F.; Carrey, J.; Lachaize, S.; Respaud, M. ; Chaudret, B. 2012. A simple chemical route toward monodisperse iron carbide nanoparticles displaying tunable magnetic and unprecedented hyperthermia properties. *Nano Lett.* 12, 4722-4728 (DOI : 10.1021/nl302160d)

[43] Dumestre, F.; Chaudret, B.; Amiens, C.; Renaud, P.; Fejes, P. 2004 Superlattices of iron nanocubes synthesized from Fe[N(SiMe3)2]2. *Science*, 303, 821-823 (DOI : 10.1126/science.1092641)

[44] Lacroix, L.-M.; Lachaize, S.; Falqui, A.; Respaud, M.; Chaudret, B. 2009 Iron nanoparticle growth in organic superstructures. *J. Am. Chem. Soc.*, 131, 549-557 (DOI : 10.1021/ja805719c)

[45] Meffre A. ; Lachaize, S.; Gatel, C.; Respaud, M. ; Chaudret, B. 2011 Use of long chain amine as a reducing agent for the synthesis of high quality monodisperse iron(0) nanoparticles. *J. Mater. Chem.*, 21, 13464-13469 (DOI : 10.1039/C1JM12127H)

[46] Puntes, V. F.; Krishnan, K. M.; Alivisatos, A. P. 2001. Colloidal nanocrystal shape and size control : the case of cobalto. *Science*, 291, 2115-2117 (DOI : 10.1126/science.1057553)

[47] Keng, P. Y. ; Shim, I. ; Korth, B. D.; Douglas, J. F.; Pyun, J. 2009. Synthesis and self assembly of polymer-coated ferromagnetic nanoparticles. *ACS Nano*, 1, 279-292 (DOI : 10.1021/nn7001213)

[48] Osuna, J.; de Caro, D.; Amiens, C.; Chaudret, B.; Snoeck, E.; Respaud, M.; Broto, J.-M.; Fert, A. 1996. Synthesis, characterization, and magnetic properties of cobalt nanoparticles from an organometallic precursor. *J. Phys. Chem.*, 100, 14571-14574 (DOI : 10.1021/jp961086e)

[49] Sun, S.; Murray, C. B. 1999 Synthesis of monodisperse cobalt nanocrystals and their assembly into magnetic superlattices. *J. Appl. Phys.* 85, 4325-4330 (DOI : 10.1063/1.370357)

[50] Soumare, Y. ; Garcia, C. ; Maurer, T. ; Chaboussant, G. ; Ott, F. ; Fiévet, F. ; Piquemal, J.-Y. ; Viau, G. 2009. Kinetically controlled synthesis of hexagonally close-packed cobalt nanorods with high magnetic coercivity. *Adv. Funct. Mater.* 19, 1971-1977 (DOI : 10/1002/adfm.200800822)

[51] Dumestre F. ; Chaudret, B. ; Amiens, C. ; Respaud, M. ; Fejes, P. ; Renaud, P. ; Zurcher, P. 2003. Unprecedented crystalline super-lattices of monodisperse cobalt nanorods. *Angew. Chem. Int. Ed.*, 42, 5213-5216 (DOI : 10.1002/anie.200352090)

[52] Liakakos, N. ; Cormary, B. ; Li, X. ; Lecante, P.; Respaud, M.; Maron, L.; Falqui, A.; Genovese, A.; Vendier, L.; Koïnis, S.; Chaudret, B. ; Soulantica, K. 2012. The big impact of a small detail : cobalt nanocrystal polymorphism as a result of precursor addition rate during stock solution preparation. *J. Am. Chem. Soc.* 134, 17922-17931 (DOI : 10.1021/ja304487b)

[53] Lacroix, L.-M.; Lachaize, S.; Carrey, J.; Respaud, M.; Chaudret, B. 2011. Iron nanoparticles with tuneable sizes for hyperthermia applications. L'*Act. Chim.*. 351, 28-35.

[54] Desvaux, C.; Amiens, C.; Fejes, P.; Renaud, P.; Respaud, M.; Lecante, P.; Snoeck, E. ; Chaudret, B. 2005 Multimillimetre-large superlattices of air-stable iron-cobalt nanoparticles. *Nat. Mater.*, 4, 750-753 (DOI : 10.1038/nmat1480)

[55] Wang, C.; Peng, S.; Lacroix, L.-M.; Sun, S. 2009 Synthesis of high magnetic moment CoFe nanoparticles via interfacial diffusion in core/shell structured Co/Fe nanoparticles. *Nano Res.*, 2, 380-385 (DOI : 10.1007/s12274-009-9037-4)

[56] Ogawa, T.; Takano, H.; Kura, H.; Takahashi, M. 2012 Synthesis of Fe-Co nanoparticles with high saturation magnetization by low temperature post-annealing. *J. Appl. Phys.* 111, 07B533 (DOI :10.1063/1.3679027)

[57] Sun, S. ; Murray, C. B.; Weller, D.; Folks, L.; Moser, A. 2000 Monodisperse FePt nanoparticles and ferromagnetic FePt nanocrystal superlattices. *Science* 287, 1989-1992 (DOI : 10.1126/science.287.5460.1989)

[58] Sun, S. 2006. Recent Advances in Chemical Synthesis, Self-Assembly, and Applications of FePt Nanoparticles. *Adv. Mater.* 18, 393-403 (DOI: 10.1002/adma.200501464)

[59] Gao, J. ; Liang, G. ; Cheung, J. S.; Pan, Y.; Kuang, Y.; Zhao, F.; Zhang, B.; Zhang, X.; Wu, E. X.; Xu, B. 2008 Multifunctional Yolk-Shell nanoparticles : a potential MRI contrast and anticancer agent. *J. Am. Chem. Soc.* 130, 11828-11833 (DOI : 10.1021/ja803920b)

[60] Pei, W.; Kakibe, S.; Ohta, I.; Takahashi, M. 2005. Controlled monodisperse Fe nanoparticles synthesized by chemical method. *IEEE Trans. Magn.* 41, 3391-3393 (DOI : 10.1109/TMAG.2005.855207)

[61] Shavel, A.; Rodriguez-Gonzalez, B.; Spasova, M;. Farle, M.; Liz-Marzan, L. M. 2007. Synthesis and characterization of iron/iron oxide core/shell nanocubes. *Adv. Funct. Mater.* 17, 3870-3876 (DOI: 10.1002/adfm.200700494)

[62] Guo, Z.; Henry, L. L.; Palshin, V.; Podlaha, E. J. 2006. Synthesis of poly(methyl methacrylate) stabilized colloidal zero-valence metallic nanoparticles. *J. Mater. Chem.*, 16, 1772-1777 (DOI : 10.1039/b515565g)

[63] Chaubey, G. S.; Barcena, C.; Poudyal, N.; Rong, C.; Gao, J.; Sun, S.; Liu, J. P. 2007. Synthesis and stabilization of FeCo Nanoparticles. *J. Am. Chem. Soc.* 129, 7214-7215 (DOI : 10.1021/ja0708969)

[64] Elkins, K. E.; Chaubey, G. S. ; Nandwana, V. ; Liu, J. P. 2008. A novel approach to synthesis of FePt magnetic nanoparticles. *J. Nano. Res*., 1, 23-30 (DOI : 10.4028/www.scientific.net/JNanoR.1.23)

[65] Sun, S.; Anders, S.; Thomson, T.; Baglin, J. E. E.; Toney, M. F.; Hamann, H. F.; Murray, C. B.; Terris, B. D. 2003. Controlled synthesis and assembly of FePt nanoparticles. *J. Phys. Chem. B*, 107, 5419-5425 (DOI : 10.1021/jp027314o)

[66] Pansare, V. J.; Hejazi, S.; Faenza, W. J.; Prud'homme, R. K. 2012 Review of Long-Wavelength Optical and NIR Imaging Materials: Contrast Agents, Fluorophores, and Multifunctional Nano Carriers, *Chem. Mater*., 24, 812−827 (DOI: 10.1021/cm2028367).

[67] Weissleder, R. 2001 A clearer vision for *in vivo* imaging, *Nat. Biotechnol.*, 19, 316-317. (DOI : 10.1038/86684)

[68] Frangioni, J. V. 2003 In vivo near-infrared fluorescence imaging, *Curr. Opin. Chem. Biol.*, 7:626–634 (DOI 10.1016/j.cbpa.2003.08.007)

[69] Resch-Genger, U.; Grabolle1, M.; Cavaliere-Jaricot, S.; Nitschke, R.; Nann T. 2008 Quantum dots versus organic dyes as fluorescent labels, *Nature Meth.*, 5, 763–775 (DOI: 10.1038/ nmeth.1248)

[70] Berlier, J. E.; Rothe, A.; Buller, G.; Bradford, J.; Gray, D. R.; Filanoski, B. J.; Telford, W. G.; Yue, S.; Liu, J.; Cheung, C.-Y.; Chang, W.; Hirsch, J. D.; Beechem, J. M.; Haugland, R. P.; Haugland, R. P. 2003 Quantitative Comparison of Long-wavelength Alexa Fluor Dyes to Cy Dyes: Fluorescence of the Dyes and Their Bioconjugates. *J. Histochem. Cytochem.* 51, 1699–1712 (DOI: 10.1177/002215540305101214)

[71] Aswathy, R. G.; Yoshida, Y.; Maekawa, T.; Kumar D. S. 2010 Near-infrared quantum dots for deep tissue imaging, *Anal. Bioanal. Chem.*, 397, 1417–1435 (DOI: 10.1007/s00216-010-3643-6).

[72] Shan, J.; Uddi, M.; Wei, R.; Yao, N.; Ju Y. 2010 The Hidden Effects of Particle Shape and Criteria for Evaluating the Upconversion Luminescence of the Lanthanide Doped Nanophosphors, *J. Phys. Chem. C*, 114, 2452–2461 (DOI: 10.1021/jp908976n).

[73] Chatterjee, D. K.; Gnanasammandhan, M. K.; Zhang Y. 2010 Small Upconverting Fluorescent Nanoparticles for Biomedical Applications, *Small*, 6, 2781–2795 (DOI: 10.1002/smll.201000418).

[74] Luo, Z.; Yuan, X.; Yu, Y.; Zhang, Q.; Leong, D. T.; Lee, J. Y.; Xie J. 2012 From Aggregation-Induced Emission of Au(I)−Thiolate Complexes to Ultrabright Au(0)@Au(I)−Thiolate Core−Shell Nanoclusters, *J. Am. Chem. Soc.*, 134 (40), 16662–16670 (DOI: 10.1021/ja306199p).

[75] Baba, K.; Nishida, K. 2012 Single-Molecule Tracking in Living Cells Using Single Quantum Dot Applications *Theranostics*, 2, 655–667 (DOI: 10.7150/thno.3890)

[76] Alivisatos, A. P. 1996 Perspectives on the Physical Chemistry of Semiconductor Nanocrystals *J. Phys. Chem.*, 100, 13226–13239 (DOI: 10.1021/jp9535506).

[77] de Mello Donega, C. 2011 Synthesis and properties of colloidal heteronanocrystals. *Chem. Soc. Rev.*, 40, 1512–1546 (DOI: 10.1039/c0cs00055h).

[78] Smith, A. M.; Nie, S. 2010 Semiconductor Nanocrystals: Structure, Properties, and Band Gap Engineering *Acc. Chem. Res.*, 43, 190 –200 (DOI: 10.1021/ar9001069).

[79] Bailey, R. E.; Nie, S. 2003 Alloyed semiconductor quantum dots: tuning the optical properties without changing the particle size, *J. Am. Chem. Soc.*, 125, 7100-7106 (DOI: 10.1021/ja035000o).

[80] Gaponik, N.; Rogach, A. L. 2008 Aqueous Synthesis of Semiconductor Nanocrystals in Semiconductor Nanocrystals Quantum Dots, Ed. Rogach, A. L. SpringerWienNewYork.

[81] Xue, B.; Deng, D.-W.; Cao, J.; Liu, F.; Li, X.; Akers, W.; Achilefu S.; Gu, Y.-Q. 2012 Synthesis of NAC capped near infrared-emitting CdTeS alloyed quantum dots and application for in vivo early tumor imaging *Dalton Trans.*, 41, 4935–4947 (DOI: 10.1039/c2dt12436j).
[82] Pons, T.; Lequeux, N.; Mahler, B.; Sasnouski, S.; Fragola, A.; Dubertret, B. 2009 Synthesis of Near-Infrared-Emitting, Water-Soluble CdTeSe/CdZnS Core/Shell Quantum Dots. *Chem. Mater.* 21, 1418–1424 (DOI: 10.1021/cm8027127)
[83] Harrison, M. T.; Kershaw, S. V.; Burt, M. G.; Eychmuller, A.; Weller, H.; Rogach A. L. 2000 Wet chemical synthesis and spectroscopic study of CdHgTe nanocrystals with strong near-infrared luminescence *Materials Science and Engineering* B69–70, 355–360.
[84] Kovalenko, M. V.; Kaufmann, E.; Pachinger, D.; Roither, J.; Huber, M.; Stangl, J.; Hesser, G.; Schaffler, F.; Heiss, W. 2006 Colloidal HgTe Nanocrystals with Widely Tunable Narrow Band Gap Energies: From Telecommunications to Molecular Vibrations *J. Am. Chem. Soc.*, 128, 3516-3517 (DOI: 10.1021/ja058440j)
[85] Cademartiri, L.; Montanari, E.; Calestani, G.; Migliori, A.; Guagliardi, A.; Ozin, G. A. 2006 Size-Dependent Extinction Coefficients of PbS Quantum Dots *J. Am. Chem. Soc.*, 128, 10337-10346 (DOI: 10.1021/ja063166u).
[86] Hines, M. A.; Scholes, G. D. 2003 Colloidal PbS Nanocrystals with Size-Tunable Near-Infrared Emission: Observation of Post-Synthesis Self-Narrowing of the Particle Size Distribution *Adv. Mater.*, 15, 1844–1849 (DOI: 10.1002/adma.200305395).
[87] Akhtar, J.; Afzaal, M.; Banski, M.; Podhorodecki, A.; Syperek, M.; Misiewicz, J.; Bangert, U.; Hardman, S. J. O.; Graham, D. M.; Flavell, W. R.; Binks, D. J.; Gardonio, S.; O'Brien, P. 2011 Controlled Synthesis of Tuned Bandgap Nanodimensional Alloys of PbS_xSe_{1-x}, *J. Am. Chem. Soc.*, 133, 5602–5609 (DOI: 10.1021/ja200750s).
[88] Moreels, I.; Lambert, K.; De Muynck, D.; Vanhaecke, F.; Poelman, D.; Martins, J. C.; Allan, G.; Hens, Z. 2007 Composition and Size-Dependent Extinction Coefficient of Colloidal PbSe Quantum Dots *Chem. Mater.*, 19, 6101–6106 (DOI: 10.1021/cm071410q).
[89] Murphy, J. E.; Beard, M. C.; Norman, A. G.; Ahrenkiel, S. P.; Johnson, J. C.; Yu, P.; Micic, O. I.; Ellingson, R. J.; Nozik, A. J. 2006 PbTe Colloidal Nanocrystals: Synthesis, Characterization, and Multiple Exciton Generation *J. Am. Chem. Soc.*, 128, 3241–3247 (DOI: 10.1021/ja0574973).
[90] Xie, R.; Battaglia, D.; Peng, X. 2007 Colloidal InP Nanocrystals as Efficient Emitters Covering Blue to Near-Infrared *J. Am. Chem. Soc.*, 128, 15432–15433 (DOI: 10.1021/ja076363h).
[91] Xie, R.; Peng, X. 2009 Synthesis of Cu-Doped InP Nanocrystals (d-dots) with ZnSe Diffusion Barrier as Efficient and Color-Tunable NIR Emitters *J. Am. Chem. Soc.*, 131, 10645–10651 (DOI: 10.1021/ja903558r).
[92] Kim, S.-W.; Zimmer, J. P.; Ohnishi, S.; Tracy, J. B.; Frangioni, J. V.; Bawendi, M. G. 2005 Engineering $InAs_xP_{1-x}$/InP/ZnSe III-V Alloyed Core/Shell Quantum Dots for the Near-Infrared *J. Am. Chem. Soc.*, 127, 10526–10532 (DOI: 10.1021/ja0434331).
[93] Xie, R.; Peng, X. 2008 Synthetic Scheme for High-Quality InAs Nanocrystals Based on Self-Focusing and One-Pot Synthesis of InAs-Based Core–Shell Nanocrystals, *Angew. Chem. Int. Ed.*, 47, 7677–7680 (DOI: 10.1002/anie.200802867).
[94] Xie, R.; Zhang, J.; Zhao, F.; Yang, W.; Peng, X. 2010 Synthesis of Monodisperse, Highly Emissive, and Size-Tunable Cd_3P_2 Nanocrystals, *Chem. Mater.*, 22, 3820–3822 (DOI: 10.1021/cm1008653).
[95] Harris, D. K.; Allen, P. M.; Han, H.-S.; Walker, B. J.; Lee, J.; Bawendi, M. G. 2011 Synthesis of Cadmium Arsenide Quantum Dots Luminescent in the Infrared *J. Am. Chem. Soc.*, 133, 4676–4679 (DOI: 10.1021/ja1101932).

[96] Xie, R.; Rutherford, M.; Peng, X. 2009 Formation of High-Quality I-III-VI Semiconductor Nanocrystals by Tuning Relative Reactivity of Cationic Precursors *J. Am. Chem. Soc.*, 131, 5691–5697 (DOI: 10.1021/ja9005767).
[97] Cassette, E.; Pons, T.; Bouet, C.; Helle, M.; Bezdetnaya, L.; Marchal, F.; Dubertret, B. 2010 Synthesis and Characterization of Near-Infrared Cu-In-Se/ZnS Core/Shell Quantum Dots for In vivo Imaging *Chem. Mater.*, 22, 6117–6124 (DOI: 10.1021/cm101881b).
[98] Ruddy, D. A.; Johnson, J. C.; Smith, E. R.; Neale, N. R. 2010 Size and Bandgap Control in the Solution-Phase Synthesis of Near-Infrared-Emitting Germanium Nanocrystals *ACS Nano*, 4, 7459–7466 (DOI: 10.1021/nn102728u).
[99] Lee, D. C.; Pietryga, J. M.; Robel, I.; Werder, D. J.; Schaller, R. D.; Klimov V. I. 2009, Colloidal Synthesis of Infrared-Emitting Germanium Nanocrystals, *J. Am. Chem. Soc.*, 131, 3436–3437 (DOI: 10.1021/ja809218s).
[100] Jiang, P.; Zhu, C.-N.; Zhang, Z.-L.; Tian, Z.-Q.; Pang, D.-W. 2012 Water-soluble Ag_2S quantum dots for near-infrared fluorescence imaging in vivo. *Biomaterials*, 33, 5130−5135 (DOI: 10.1016/j.biomaterials.2012.03.059).
[101] Yarema, M.; Pichler, S.; Sytnyk, M.; Seyrkammer, R.; Lechner, R. T.; Fritz-Popovski, G.; Jarzab, D.; Szendrei, K.; Resel, R.; Korovyanko, O.; Loi, M. A.; Paris, O.; Hesser, G.; Heiss W. 2011. Infrared Emitting and Photoconducting Colloidal Silver Chalcogenide Nanocrystal Quantum Dots from a Silylamide-Promoted Synthesis. *ACS Nano*, 5, 3758–3765 (DOI: 10.1021/nn2001118)
[102] Reiss, P.; Protière, M.; Li, L. 2009 Core/Shell Semiconductor Nanocrystals, *Small*, 5, 154–168 (DOI: 10.1002/smll.200800841).
[103] Gaponik, N.; Hickey, S. G.; Dorfs, D.; Rogach, A. L.; Eychmüller, A. 2010 Progress in the Light Emission of Colloidal Semiconductor Nanocrystals, *Small*, 6, 1364–1378 (DOI: 10.1002/smll.200902006).
[104] Wang, C.; Gao, X.; Su X. 2010 In vitro and in vivo imaging with quantum dots, *Anal. Bioanal. Chem.*, 397, 1397–1415 (DOI: 10.1007/s00216-010-3481-6).
[105] Murray, C. B.; Norris, D. J.; Bawendi, M. G. 1993 Synthesis and Characterization of Nearly Monodisperse CdE (E = S, Se, Te) Semiconductor Nanocrystallites, *J. Am. Chem. Soc.*, 115, 8706–8715 (DOI: 10.1021/ja00072a025).
[106] Peng, Z. A.; Peng X. 2001 Formation of High-Quality CdTe, CdSe, and CdS Nanocrystals Using CdO as Precursor, *J. Am. Chem. Soc.*, 123, 183–184 (DOI: 10.1021/ja003633m).
[107] Yu, W.; Peng X. 2002 Formation of High-Quality CdS and Other II–VI Semiconductor Nanocrystals in Noncoordinating Solvents: Tunable Reactivity of Monomers, *Angew. Chem. Int. Ed.*, 41, 2368–2371 (DOI: 10.1002/1521-3773).
[108] Siy, J. T.; Brauser E. M.; Bartl M. H. 2011 Low-temperature synthesis of CdSe nanocrystal quantum dots, *Chem. Commun.*, 2011,47, 364–366 (DOI: 10.1039/c0cc02304c).
[109] Murray, C. B.; Sun, S. H.; Gaschler, W.; Doyle, H.; Betley, T. A.; Kagan, C. R. 2001 Colloidal synthesis of nanocrystals and nanocrystal superlattices *IBM J. Res. Dev.*, 45, 47–56.
[110] Lu, W. G.; Fang, J. Y.; Stokes, K. L.; Lin, J. 2004 Shape Evolution and Self Assembly of Monodisperse PbTe Nanocrystals *J. Am. Chem. Soc.*, 126, 11798–11799. (DOI: 10.1021/ja0469131).
[111] Rogach, A. L.; Eychmüller, A.; Hickey, S. G.; Kershaw, S. V. 2007 Infrared-Emitting Colloidal Nanocrystals: Synthesis, Assembly, Spectroscopy, and Applications, *Small*, 3, 536–557 (DOI: 10.1002/smll.200600625).
[112] Ojo, W.-S.; Xu, S.; Delpech, F.; Nayral, C.; Chaudret B. 2012 Room-Temperature Synthesis of Air-Stable and Size-Tunable Luminescent ZnS-Coated Cd_3P_2 Nanocrystals with High Quantum Yields *Angew. Chem. Int. Ed.*, 51, 738 –741 (DOI: 10.1002/anie.201104864).

[113] Bottrill M.; Green M. 2011 Some aspects of quantum dot toxicity *Chem. Commun.*, 47, 7039–7050 (DOI: 10.1039/c1cc10692a).
[114] Antunez , P. D.; Buckley J. J.; Brutchey R. L. 2011 Tin and germanium monochalcogenide IV–VI semiconductor nanocrystals for use in solar cells. *Nanoscale*, 3, 2399–2411 (DOI: 10.1039/C1NR10084J)
[115] Kovalenko, M.V.; Heiss, W.; Shevchenko, E.V.; Lee, J.-S.; Schwinghammer, H.; Alivisatos, A.P.; Talapin, D.V. 2007 SnTe Nanocrystals: A New Example of Narrow-Gap Semiconductor Quantum Dots. *J. Am. Chem. Soc.*, 129, 11354–11355 (DOI: 10.1021/ja074481z).
[116] Micic, O. I.; Curtis, C. J.; Jones, K. M.; Sprague, J. R.; Nozik, A. J. 1994 Synthesis and Characterization of InP Quantum Dots. *J. Phys. Chem.*, 98, 4966–4969 (DOI: 10.1021/j100070a004).
[117] Battaglia D.; Peng, X. 2002 Formation of High Quality InP and InAs Nanocrystals in a Noncoordinating Solvent. *Nano Lett.*, 2, 1027–1030 (DOI: 10.1021/nl025687v).
[118] Cros-Gagneux, A.; Delpech, F.; Nayral, C.; Cornejo, A.; Coppel, Y.; Chaudret, B. 2010 Surface Chemistry of InP Quantum Dots: A Comprehensive Study. *J. Am. Chem. Soc.*, 132, 18147–18157 (DOI: 10.1021/ja104673y).
[119] Guzelian, A. A.; Banin, U.; Kadavanich, A. V.; Peng, X.; Alivisatos A. P. 1996 Colloidal chemical synthesis and characterization of InAs nanocrystal quantum dots. *Appl. Phys. Lett.* 69, 1432–1434 (DOI: 10.1063/1.117605).
[120] Choi, H. S.; Ipe, B. I.; Misra, P.; Lee, J. H.; Bawendi, M. G.; Frangioni, J. V. 2009 Tissue- and Organ-Selective Biodistribution of NIR Fluorescent Quantum Dots, *Nano Lett.*, 9, 2354–2359 (DOI: 10.1021/nl900872r).
[121] Malik, M. A.; O'Brien, P.; Revaprasadu, N. 1999 A Novel Route for the Preparation of CuSe and CuInSe2 Nanoparticles *Adv. Mater.*, 11, 1441–1444 (DOI: 10.1002/(SICI)1521-4095(199912)).
[122] Castro, S. L.; Bailey, S. G.; Raffaelle R. P.; Banger, K. K.; Hepp A. F. 2003 Nanocrystalline Chalcopyrite Materials (CuInS2 and CuInSe2) via Low-Temperature Pyrolysis of Molecular Single-Source Precursors, *Chem. Mater.*, 15, 3142–3147 (DOI: 10.1021/cm034161o)
[123] Zhong, H.; Li, Y.; Ye, M.; Zhu, Z.; Zhou, Y.; Yang, C.; Li, Y. 2007 A facile route to synthesize chalcopyrite $CuInSe_2$ nanocrystals in non-coordinating Solvent, *Nanotechnology*, 18, 025602 (DOI: 10.1088/0957-4484/18/2/025602).
[124] Lambert, T. N.; Andrews, N. L.; Gerung, H.; Boyle, T. J.; Oliver, J. M.; Wilson, B. S.; Han S. M. 2007 Water-Soluble Germanium(0) Nanocrystals: Cell Recognition and Near-Infrared Photothermal Conversion Properties, *Small*, 3, 691 – 699 (DOI: 10.1002/smll.200600529).
[125] Du, Y.; Xu, B.; Fu, T.; Cai, M.; Li, F.; Zhang, Y.; Wang, Q. 2010 Near-Infrared Photoluminescent Ag_2S Quantum Dots from a Single Source Precursor, *J. Am. Chem. Soc.*, 132, 1470–1471 (DOI: 10.1021/ja909490r).
[126] Gu, Y.-P.; Cui, R.; Zhang, Z.-L.; Xie, Z.-X.; Pang D.-W. 2012 Ultrasmall Near-Infrared Ag_2Se Quantum Dots with Tunable Fluorescence for in Vivo Imaging. *J. Am. Chem. Soc.*, 134, 79−82 (DOI: 10.1021/ja2089553)
[127] Hocaoglu, I.; Cizmeciyan, M. N.; Erdem, R.; Ozen, C.; Kurt, A.; Sennarogluad, A.; Acar H. Y. 2012 Development of highly luminescent and cytocompatible near-IR-emitting aqueous Ag_2S quantum dots *J. Mater. Chem.*, 22, 14674–14681 (DOI: 10.1039/c2jm31959d).
[128] Tian, Z.-Q.; Zhu, C.-N.; Zhang, Z.-L. 2012 Emission-Tunable Near-Infrared Ag_2S Quantum Dots, *Chem. Mater*. 24, 3−5 (DOI: 10.1021/cm202543m).

[129] Peng, S. ; Wang, C. ; Xie, J. ; Sun, S. 2006. Synthesis and stabilization of monodisperse Fe nanoparticles. *J. Am. Chem. Soc.* 128, 10676-10677 (DOI : 10.1021/ja063969h)
[130] Gao, J. ; Liang, G. ; Zhang, B. ; Kuang, Y. ; Zhang, X.; Xu, B. 2007. FePt@CoS2 yolk-shell nanocrystals as a potent agent to kill HeLa cells. *J. Am. Chem. Soc.* 129. 1428-1433 (DOI : 10.1021/ja067785e)
[131] Shubayev, V. I.; Pisanic II, T. R.; Jin, S. 2009. Magnetic nanoparticles for theragnostics. *Adv. Drug. Deliv. Rev.* 61, 467-477 (DOI : 10.1016/j.addr.2009.03.007)
[132] Dreaden, E. C. ; Alkilany, A. M.; Huang, X.; Murphy, C. J.; El-Sayed, M. A. 2012. The golden age: gold nanoparticles for biomedicine. *Chem. Soc. Rev*. 41, 2740-2779 (DOI : 10.1039/c1cs15237h)
[133] Lee, W.-R.; Kim, M. G.; Choi, J.-R.; Park, J.-I.; Ko, S. J.; Oh, S. J.; Cheon, J. 2005. Redox transmetalation process as a generalized synthetic strategy for core shell magnetic nanoparticles. *J. Am. Chem. Soc.*, 127, 16090-16097 (DOI : 10.1021/ja053659j)
[134] Chaudhuri, R. G. ; Paria, S. 2012. Core/shell nanoparticles : classes, properties, synthesis mechanisms, characterization, and applications. *Chem. Rev.* 112, 2373-2433 (DOI : 10.1021/cr100449n)
[135] Wetz, F.; Soulantica, K.; Falqui, A.; Respaud, M.; Snoeck, E.; Chaudret, B. 2007. Hybrid Co-Au nanorods: controlling Au nucleation and location. *Angew. Chem. Int. Ed.*, 46, 7079-7081 (DOI: 10.1002/anie.200702017)
[136] Schrand, A. M.; Rahman, M. F.; Hussain, S. M.; Schlager, J. J.; Smith, D. A.; Syed, A. F. 2010. Metal-based nanoparticles and their toxicity assessment. *WIREs Nanomed. Nanobiotech*. 2, 544-568 (DOI : 10.1002/wnan.103)
[137] Guerrero-Martinez, A.; Perez-Juste, J.; Liz-Marzan, L. M. 2010. Recent progress on silica coating of nanoparticles and related nanomaterials, *Adv. Mater.* 22, 1182-1195 (DOI : 10.1002/adma.200901263)
[138] El Hawi, N.; Nayral, C.; Delpech, F.; Coppel, Y.; Cornejo, A.; Castel, A.; Chaudret, B. 2009. Silica nanoparticles Brown and stabilized in organic nonalcoholic media. *Langmuir*. 25, 7540-7546 (DOI : 10.1021/la9011789)
[139] F. Delpech, C. Nayral, N. El Hawi *Manufacturing process for silica-coated metal nanoparticles*
International Patent PCT, Patent number: WO 2009071794, Filing date: 18.11.2008
[140] Li, L.; Protière, M.; Reiss, P. 2008 Economic Synthesis of High Quality InP Nanocrystals Using Calcium Phosphide as the Phosphorus Precursor, *Chem. Mater.*, 20, 2621–2623 (DOI: 10.1021/cm7035579).
[141] Chen, X.; Lou, Y.; Samia, A. C.; Burda C. 2003 Coherency Strain Effects on the Optical Response of Core/Shell Heteronanostructures *Nano Lett.*, 43, 799–803 (DOI: 10.1021/nl034243b).
[142] Ivanov, S. A.; Piryatinski, A.; Nanda, J.; Tretiak, S.; Zavadil, K. R.; Wallace, W. O.; Werder, D.; Klimov, V. I. 2007 Type-II Core/Shell CdS/ZnSe Nanocrystals: Synthesis, Electronic Structures, and Spectroscopic Properties *J. Am. Chem. Soc.*, 129, 11708-11719 (DOI: 10.1021/ja068351m).
[143] Kim, S.; Fisher, B.; Eisler, H. J.; Bawendi, M. 2003 Type-II Quantum Dots: CdTe/CdSe(Core/Shell) and CdSe/ZnTe(Core/Shell) Heterostructures *J. Am. Chem. Soc.*, 125, 11466–11467 (DOI: 10.1021/ja0361749).
[144] Mahler, B.; Spinicelli, P.; Buil, S.; Quelin, X.; Hermier, J. P..; Dubertret, B. 2008 Towards non-blinking colloidal quantum dots. *Nat. Mater.* 7, 659–664 (DOI: 10.1038/nmat2222).
[145] Wang, X.; Ren, X.; Kahen, K.; Hahn, M. A.; Rajeswaran, M.; Maccagnano-Zacher, S.; Silcox, J.; Cragg, G. E.; Efros, A. L.; Krauss T. D.2009 Non-blinking semiconductor nanocrystals. *Nature*, 459, 686–689 (DOI: 10.1038/nature08072).

[146] Medintz, I. L.; Uyeda, H. T.; Goldman, E. R.; Mattoussi, H. 2005 Quantum dot bioconjugates for imaging, labelling and sensing, *Nature Mater.*, 4, 435-446 (DOI : 10.1021/ja054630i)
[147] Basiruddin, S. K.; Saha, A.; Pradhan, N.; Jana, N. R. 2010. Advances in coating chemistry in deriving soluble functional nanoparticle. *J. Phys. Chem. C*. 114, 11009-11017 (DOI : 10.1021/jp100844d)
[148] Breus, V. V.; Heyes, C. D.; Nienhaus, G. U. 2007 Quenching of CdSe/ZnS Core/Shell Quantum Dot Luminescence by Water-Soluble Thiolated Ligands. *J. Phys. Chem. C*, 111, 18589–18594 (DOI: 10.1021/jp075848p).
[149] Yong, K.-T.; Ding, H.; Roy, I.; Law, W.-C.; Bergey, E. J.; Maitra, A.; Prasad, P. N. 2009 Imaging Pancreatic Cancer Using Bioconjugated InP Quantum Dots. *ACS Nano*, 3, 502–510 (DOI: 10.1021/nn8008933).
[150] Tamang, S.; Beaune, G.; Texier, I.; Reiss, P. 2011 Aqueous Phase Transfer of InP/ZnS Nanocrystals Conserving Fluorescence and High Colloidal Stability. *ACS Nano*, 5, 9392–9402 (DOI: 10.1021/nn203598c).
[151] Tong, S. ; Hou, S. ; Zheng, Z. ; Zhou, J. ; Bao, G. 2010. Coating optimization of superparamagnetic iron oxide nanoparticles for high T2 relaxivity. *Nano Lett.* 10, 4607-4613 (DOI : 10.1021/nl102623x)
[152] Soo Choi, H.; Liu, W.; Misra, P.; Tanaka, E.; Zimmer, J. P.; Itty Ipe, B.; Bawendi, M. G.; Frangioni, J. V. 2007. Renal clearance of quantum dots. *Nat. Biotech.* 25, 1165-1170 (.
[153] Wang, M. ; Thanou, M. 2010. Targeting nanoparticles to cancer. *Pharmacol. Res.*, 62, 90-99 (DOI : 10.1016/j.phrs.2010.03.005)
[154] Hak, S.; Hegelsen, E.; Hektoen, H. H.; Huuse, E. M.; Jarzyna, P. A.; Mulder, W. J. M.; Haraldseth, O.; de Lange Davies, C. 2012. The effect of nanoparticle polyethylene glycol surface density on ligand-directed tumor targeting studied in vivo by dual modality imaging. *ACS Nano*, 6, 5648-5658 (DOI : 10.1021/nn301630n)
[155] Lee, H. ; Lee, E.; Kim, D. K.; Jang, N. K.; Jeong, Y. Y.; Jon, S. 2006. Antibiofouling polymer-coated superparamagnetic iron oxide nanoparticles as potential magnetic resonance contrast agents for in vivo cancer imaging. *J. Am. Chem. Soc.* 128, 7383-7389 (DOI : 10.1021/ja061529k)
[156] Wilhelm, C.; Gazeau, F. 2008. Universal cell labelling with anionic magnetic nanoparticles, *Biomater.*, 29, 3161-3174 (DOI : 10.1016/j.biomaterials.2008.04.016)
[157] Villanueva, A.; Canete, M.; Roca, A. G.; Calero, M.; Veintemillas-Verdaguer, S.; Serna, C. J.; del Puerto Morales, M.; Miranda, R. 2009. The influence of surface functionalization on the enhanced internalization of magnetic nanoparticles in cancer cells, *Nanotech.*, 20, 115103 (DOI : 10.1088/0957-4484/20/11/115103)
[158] Sun C. ; Lee J. S.H. ; Zhang M. 2008. Magnetic nanoparticles in MR imaging and drug delivery, *Adv. Drug Del. Rev.* 60, 1252-1265 (DOI : 10.1016/j.addr.2008.03.018)
159 Chou S.-W. ; Shau Y.-H. ; Wu P.-C. ; Yang Y.-S. ; Shieh D.-B. ; Chen C.-C. 2010. In Vitro and in Vivo Studies of FePt Nanoparticles for Dual Modal CT/MRI Molecular Imaging, *J. Am. Chem. Soc.*, 132, 13270-13278 (DOI : 10.1021/ja1035013)
[160] Mattoussi, H.; Palui, G.; Na H. B. 2012 Luminescent quantum dots as platforms for probing in vitro and in vivo biological processes. *Adv. Drug. Deliv. Rev.* 64, 138–166 (DOI: 10.1016/j.addr.2011.09.011).
[161] Kim, S.; Lim, Y. T.; Soltesz, E. G.; De Grand, A. M.; Lee, J.; Nakayama, A.; Parker, J. A.; Mihaljevic, T.; Laurence, R. G.; Dor, D. M.; Cohn, L. H.; Bawendi, M. G.; Frangioni, J. V. 2004 Near-infrared fluorescent type II quantum dots for sentinel lymph node mapping *Nat. Biotechnol.* 22, 93–97 (DOI: 10.1038/nbt920).

[162] Deng, D.; Chen, Y.; Cao, J.; Tian, J.; Qian, Z.; Achilefu, S.; Gu, Y. 2012 High-Quality $CuInS_2$/ZnS Quantum Dots for In vitro and In vivo Bioimaging *Chem. Mater.* 24, 3029−3037 (DOI: 10.1021/cm3015594).
[163] Li, L.; Daou, T. J.; Texier, I.; Chi, T. T. K.; Liem, N. Q.; Reiss, P. 2009 Highly Luminescent CuInS2/ZnS Core/Shell Nanocrystals: Cadmium-Free Quantum Dots for In Vivo Imaging *Chem. Mater.* 21, 2422–2429 (DOI: 10.1021/cm900103b).
[164] Pons, T.; Pic, E.; Lequeux, N.; Cassette, E.; Bezdetnaya, L.; Guillemin, F.; Marchal, F.; Dubertret B. 2010 Cadmium-Free $CuInS_2$/ZnS Quantum Dots for Sentinel Lymph Node Imaging with Reduced Toxicity *ACS Nano*, 4, 2531–2538 (DOI: 10.1021/nn901421v).
[165] Park, J.; Dvoracek, C.; Lee, K. H.; Galloway, J. F.; Bhang, H.-E. C.; Pomper, M. G.; Searson, P. C. 2011 CuInSe/ZnS Core/Shell NIR Quantum Dots for Biomedical Imaging *Small*, 7, 3148–3152 (DOI: 10.1002/smll.201101558).
[166] Gao, J.; Chen, K.; Luong, R.; Bouley, D. M.; Mao, H.; Qiao, T.; Gambhir, S. S.; Cheng, Z. 2012 A Novel Clinically Translatable Fluorescent Nanoparticle for Targeted Molecular Imaging of Tumors in Living Subjects *Nano Lett.* 12, 281−286 (DOI: 10.1021/nl203526f).
[167] Jarzyna, P. A. ; Gianella, A. ; Skajaa, T. ; Knudsen, G.; Deddens, L. H.; Cormode, D. P.; Fayad, Z. A.; Mulder, W. J. M. 2010. Multifunctional imaging nanoprobes. *WIREs Nanomed Nanobiotech*., 2, 138-150 (DOI : 10.1002/wnan.72)
[168] Hao, R. ; Wing, R. ; Xu, Z. ; Hou, Y.; Gao, S.; Sun, S. 2010. Synthesis, functionalization, and biomedical applications of multifunctional magnetic nanoparticles. *Adv. Mater.* 22, 2729-2742 (DOI : 10.1002/adma.201000260)
[169] Corr, S. A.; Rakovich, Y. P.; Gun'ko, Y. K. 2008. Multifunctional magnetic-fluorescent nanocomposites for biomedical applications. *Nanoscale Res. Lett.* 3, 87-104 (DOI : 10.1007/s11671-008-9122-8)
[170] Ho, D. ; Sun, X. ; Sun, S. 2011. Monodisperse magnetic nanoparticles for theranostic applications. *Acc. Chem. Res.* 44, 875-882 (DOI : 10.1021/ar200090c)
[171] Zanella, M.; Falqui, A.; Kudera, S.; Manna, L.; Casula, M. F.; Parak, W. J. 2008. Growth of colloidal nanoparticles of group II-VI and IV-VI semiconductors on top of magnetic iron-platinum nanocrystals. *J. Mater. Chem.* 18, 4311-4317 (DOI : 10.1039/b804154g)
[172] Trinh, T. T.; Mott, D.; Thanh, N. T. K.; Maenosono, S. 2011. One-pot synthesis and characterization of well defined core-shell structure FePt@CdSe nanoparticles. *RSC Advances*, 1, 100-108 (DOI : 10.1039/c1ra00012h)
[173] Gu, H. ; Zheng, R. ; Zhang, X. ; Xu, B. 2004. Facile one-pot synthesis of bifunctional heterodimers of nanoparticles : a conjugate of quantum dot and magnetic nanoparticles. *J. Am. Chem. Soc*. 126, 5664-5665 (DOI : 10.1021/ja0496423)
[174] Maynadié, J. ; Salant, A. ; Falqui, A. ; Respaud, M. ; Shaviv, E. ; Banin, U. ; Soulantica, K. ; Chaudret, B. 2008. Cobalt growth on the tips of CdSe nanorods. *Angew. Chem. Int. Ed.* 48, 1814-1817 (DOI : 10.1002/anie.200804798)
[175] Gao, J. ; Zhang, W. ; Huang, P. ; Zhang, B.; Zhang, X.; Xu, B. 2008. Intracellular spatial control of fluorescent magnetic nanoparticles. *J. Am. Chem. Soc.* 130, 3710-3711 (DOI : 10.1021/ja7103125)
[176] Shen, J.-M. ; Guan, X.-M. ; Liu, X.-Y.; Lan, J.-F.; Cheng, T.; Zhang, H.-X. 2012. Luminescent/magnetic hybrid nanoparticles with folate-conjugated peptide composited for tumor-targeted drug delivery. *Bioconjugate Chem.* 23, 1010-1021 (DOI : 10.1021/bc300008k)
[177] Bigall, N. C.; Parak, W. J.; Dorfs, D. 2012. Fluorescent, magnetic and plasmonic-Hybrid multifunctional colloidal nano objects. *Nano Today*. 7, 282-296 (DOI : 10.1016/j.nantod.2012.06.007)
[178] Deka, S. ; Falqui, A. ; Bertoni, G. ; Sangregorio, C.; Poneti, G.; Morello, G.; De Giorgi, M.; Giannini, C.; Cingolani, R.; Manna, L.; Cozzoli, P. D. 2009. Fluorescent asymmetrically

cobalt-tipped CdSe@CdS core@shell nanorod heterostructures exhibiting room-temperature ferromagnetic behavior. *J. Am. Chem. Soc.* 131, 12817-12828 (DOI : 10.1021/ja904493c)